Ph. D. DISSERTATION

Study on light transmission in metallic nanostructures through charge redistribution mechanism

전하 재분포 메카니즘를 통한 금속 나노 구조물에서의 빛의 투과에 대한 연구

By

TAERIN CHUNG

FEBRUARY 2014

DEPARTMENT OF ELECTRICL AND
COMPUTER ENGINEERING
COLLEGE OF ENGINEERING
SEOUL NATIONAL UNIVERSITY

Abstract

Study on light transmission in metallic nanostructures through charge redistribution mechanism

TAERIN CHUNG
DEPARTMENT OF ELECTRICAL AND
COMPUTER ENGINEERING
COLLEGE OF ENGINEERING
SEOUL NATIONAL UNIVERSITY

This dissertation studies on light transmission through metallic nanostructures using induced charge distribution mechanism. When light passes through metallic nanostructures, charges in a metallic nanostructure are induced and relocated with regard to the shape, dimension, and incident polarization of state. Induced charge redistribution is mainly investigated because it directly correlates to the electric field distribution and surface current flow at a metal nanostructure. Localized surface plasmons (LSP) at a metal nanostructure are observed in an optical regime, which mean the (confined)

collective electron excitations at the interface between metallic nanostructure and surrounding dielectric. Fumbling induced charge distribution at a metal nanostructure in optical regime can lead to manipulation of the optical properties such as enhanced transmission, concentration and confinement. In case of coupled metallic nanorods where they produce localized electromagnetic field strength at the nanogap nestled between coupled metallic nanorods; enhanced local fields originate from local capacitive coupling. It results from the accumulated charges at the edge of each nanorod. Derived from this structure, plasmonic faced folded metallic nanorods are proposed by the folding and facing of metallic nanorods. Its physical dimension is designed on the basis of $\lambda_{spp}/4$.

This proposed structure presents unique induced charge redistribution models with regard to incident polarization state of light via numerical calculations. Furthermore, distinct surface current flow, called semi-circular current flow, is introduced, resulting from induced charge redistribution. Assuming that semi-circular current flow contributes to the optical properties of near- and far-field transmission, transmission characteristics passing through faced folded metallic nanorods are experimentally observed using three-dimensional holographic microscopy. This proposed structure is numerically and experimentally demonstrated. Novel route of surface current in a metallic nanostructure leads to the significant increase of degree of field intensity. It is verified with the numerical calculations based on finite difference time domain (FDTD) method, presenting the comparisons with simplified geometries. Whole beam path emanating from the proposed structure can be observed via three-dimensional holographic microscopy. Light intensity passing through the proposed structure is enhanced and more concentrated than light passing through the bare aperture, as a reference. As a result, we establish that faced folded metallic nanorods can be functionalized as a compact light concentrator accompanying with field enhancement. In addition, a current issue in

plasmonics can be resolved by the use of metallic nanostructures. A metallic nanoslit suffers from weak transmission due to the diffraction limit. To overcome this limit, metallic nanoislands are embedded inside a metallic nanoslit. It is expected that embedded metallic nanoislands act as a platform to instigate plasmonic mode. Plasmonic modes in a metallic nanoslit with the embedded metallic nanoislands are numerically observed with regard to the incident polarization state of light. It can be attributed to enhancing the intensity of transmitted light passing through a metallic nanoslit in spite of diffraction limit. Additionally, embedded metallic nanoislands can play a critical role to adjust the location of resonant wavelength in its spectrum. As a consequence, transmission enhancement passing through a metallic nanoslit with the embedded metallic nanoislands can be experimentally demonstrated.

Keywords: Plasmonics, nanophotonics, surface plasmons, optical antenna, diffraction limit, metallic nanostructure, plasmonic nanostructure

Student number: 2010-30997

List of Figures

List of Tables

Contents

Chapter 1

Introduction

1.1. Plasmonic nanostructures and their nanophotonic application

Since the early 21st century, metallic nanostructures have received much attention in a wide range of emerging technologies [1, 2]. Recent scientific breakthroughs have brought about the advance of nanofabrication techniques [3]. In particular, noble metallic nanostructures in optical regimes are able to provide exclusive properties referred to as surface plasmons or localized surface plasmons. Surface plasmons are found at the interface between the noble bulk metal and dielectric layers. It is mentioned as the coherent electron oscillations existing at the interface between metal and dielectric layer [4]. Localized surface plasmons are taken account of surface plasmons confined to nano-scale metallic nanostructures [5]. Nano-scale plasmonic structures are considered an attractive platform, as characterized by their intense and confined electromagnetic field intensity and sensitive optical behavior in response to surrounding dielectric media. They can play versatile roles in various nanophotonic applications. Efficient interconversion of propagating light and localized, enhanced fields is instrumental for advances in optical manipulation and characterization in nanometer-scale.

Typically, light is controlled by redirecting the wavefronts of propagating radiation via lenses, mirrors and diffractive elements [6]. In a similar manner, when a metallic nanorod

is illuminated by a light with an appropriate wavelength, it can resonantly enhance light emission intensity just as an antenna enhances the emission intensity of electromagnetic waves. In a microwave regime, various types of antenna have been exploited for the purpose of manipulating electromagnetic fields, as shown in Fig. 1.1.1 [7-10]. Analogous to the microwave antenna, the concept of nanoantennas for light emission has been exploited.

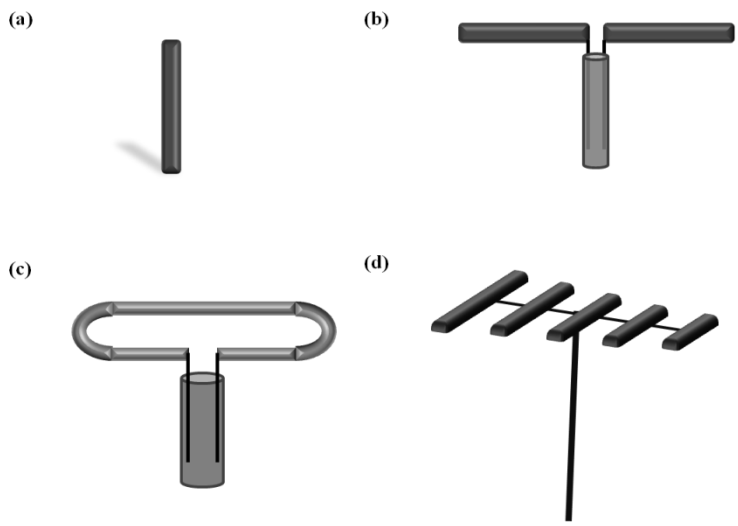

Figure 1.1.1. Various types of microwave antenna: (a) monopole antenna, (b) dipole antenna, (c) folded dipole antenna, and (d) Yagi-Uda antenna.

The fundamental type of optical antenna is the monopole antenna, which is simply designed with a metallic nanorod [11]. Coupled metallic nanorods can form a dipole antenna. Optical Yagi-Uda antennas have been shown in experiments to redirect the direction of radiating light, thus presenting directional radiation patterns [12].

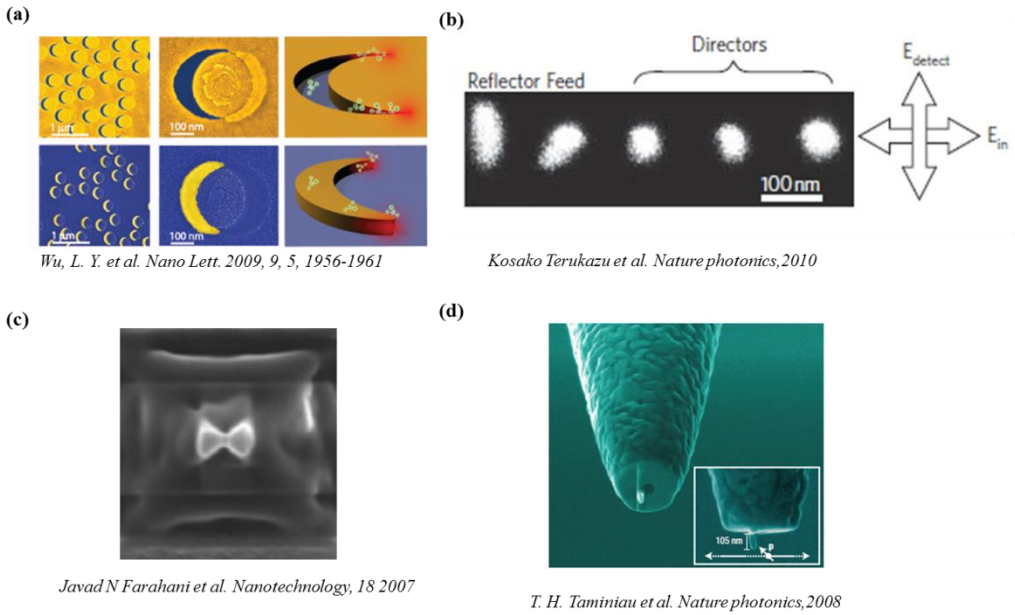

Figure 1.1.2. Representative examples of optical antenna: (a) metallic nanocrescent, (b) optical Yagi-Uda antenna, (c) bow-tie metallic nanostructure, and (d) metallic monopole antenna.

In contrast, exceptional geometries of optical antenna are plasmonic bow-tie metallic structure and metallic nanocrescents, giving rise to local intense field enhancement, as shown in Fig. 1.1.2. These optical or plasmonic antennas are capable of being the medium which can convert free-propagating optical radiation into a localized field that would interact with a sample metallic surface. In attempt to achieve significantly intense electromagnetic fields from metallic nanostructure in optical regime, tailoring the shape or dimension of a metallic nanostructure is essential.

There are several approaches on enhancing electromagnetic field strength arisen from a metallic nanostructure illuminated by the light. First, the physical dimension of a metallic nanostructure is optimized with regard to the incident wavelength, polarization state of light, materials and photonic applications. Second, a metallic nanogap nestled in coupled metallic nanostructures is attributed to enhance electromagnetic field intensity in a metallic nanostructure at optical regime. Localized capacitive coupling nestled inside a metallic nanogap helps to increase the accumulated charge density and then boost the

localized field intensity. Coupled metallic nanorods have been experimentally demonstrated, showing significant field strength at the metallic nanogap located between two metallic nanorods [13]. Local capacitor model in optical regime provides insight, presenting that the localized field intensity is linearly increased with respect to the decrease of width of a metallic nanogap [14]. In addition, a sharp edge of a metallic nanostructure allows accumulated charges to generate extreme intense localized hot spots.

Plasmonic nanostructures have been also extensively studied on the sensing platform acutely responding to the variation of bulk refractive index. Localized surface plasmons confined to the interface between metallic nanostructures and surrounding dielectric materials, are known to be sensitive to the refractive index of the dielectric medium within the penetration depth [15].

In addition, both spectral tunablity and strong enhancement of the local electric field can be obtained in plasmonic nanostructures. These properties have been employed for the development of label-free plasmonic biosensors to study the binding events between the target analyte and its corresponding receptor on a metal surface [20]. Extensive developments on metallic nanostructures have been reported in the areas of bio-imaging, bio-sensing and medical therapy [21-22] as shown in Table 1.

Table 1. Sensing characteristics of plasmonic nanostructures
(LSPR: localized surface plasmon resonance)

Nanostructure	*Wavelength*	*Structure dimension*	*Characteristics*	*Sensitivity*	*RI range*	*Ref.*
Silver spherical nanoparticles	**450 - 700 nm**	**Diameter 35 nm**	**Shape-dependent LSPR**	**161 nm/RIU**	**1 - 1.6**	**16**
Gold nano rods	**800 - 1000 nm**	**Aspect ratio 3.5 : 1 Radius 40 nm**	**Size-dependent LSPR**	**650 nm/RIU**	**1.34 -1.7**	**17**
Gold nanoring	**900 - 1500 nm**	**Diameter 150 nm Thickness 20 nm**	**Shape dependence on dielectric substrate**	**880 nm/RIU**	**1.33 – 14.2**	**18**
Gold nanocrescent	**800 - 2800 nm**	**Diameter 410 nm Deposition angle 10° Aspect ratio 4**	**Plasmon-induced electromagnetic near-field**	**879 nm/RIU**	**Streptavidin binding**	**19**
Gold nanostar	**550 – 750 nm**	**Core size 30 – 50 nm Conical tips 10 - 60 nm**	**Multiple plasmon Resonances**	**218 nm/RIU**	**1 – 1.38**	**20**

Concurrent issues in nanophotonic areas have been tried to resolve with the use of novel metallic nanostructures. Overcoming diffraction limit of light has been one of major issues for designing photonic devices in sub-wavelength scales [23]. To solve this inherent problem, optical phenomena based on surface plasmons have been considered as possible candidates. In particular, two main advantageous aspects of surface plasmons existing at the metal-dielectric interface of a metallic nanostructure have been utilized: one is a highly localized field below conventional diffraction limit, and the other is a considerably intense radiation field accompanied by it. The resonantly induced optical fields based on SPPs also lead to the applications for the use as an optical antenna in nano-scale regime as mentioned above. In an attempt to achieve directional intense radiation, phased array antenna has been widely adopted varying the phase or time delay to the elements in the microwave regime. The array of metallic nanostructures such as nanoparticles or nanoholes at optical regime has been introduced as well [24-25]. Since nanoparticles or nanoholes can act as the local scatters at visible and near-IR regime, they can also play the role of localized surface plasmon polariton source. To take advantages of antenna performance arisen from nanoparticles or various nanostructures, diverse approaches have been exploited, such as nanoparticles placed in a subwavelength metallic slit for the purpose of overcoming the diffraction limit and solving the issue of weak transmission. In contrast, there are diverse ways on focusing light within the subwavelength scale: extraordinary optical transmission (EOT) through the nanohole array, beaming phenomena via metallic gratings and super lens. Thanks to these advanced technologies, raised issues in nanophotonic applications have been untangled. These advancements can devote to flourish the technologies developed from surface plasmons as presented in Fig.1.1.3.

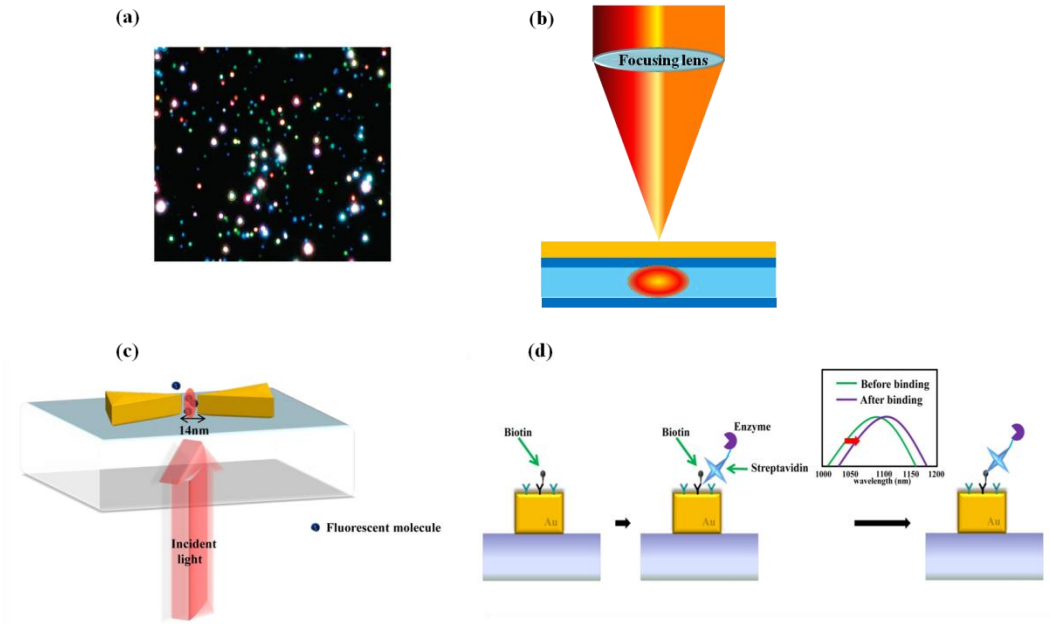

Figure 1.1.3. Nanophotonic applications with the use of a metallic nanostructure: (a) optical imaging [21], (b) optical data storage, (c) single-molecule fluorescence enhancement [22] and (d) LSPR bio-sensing[20].

1.2. Motivation of this dissertation

Surface plasmon waves are highly confined electromagnetic waves that propagate along the interface between a metal and a dielectric material via the coupling of the electrons in the noble metal. Extensive researches on surface plasmon have been performed in various areas from nanophotonic devices to biological applications. In particular, localized surface plasmon arisen from a metallic nanostructure has received much attention, representing localized, confined, and intense electromagnetic field. The unique ability of metallic nanostructures to concentrate light into the subwavelength scale allows their use in a vast area of nanophotonic technologies. Hence, the design and optimization of metallic nanostructures in optical regime is necessary to achieve extreme light concentration and enhancement. In tailoring metallic nanostructures, one of controllable factors is surface charges in a metallic structure. Surface charges are induced and

redistributed when a metallic nanostructure is excited by electromagnetic field. The redistribution mechanism of induced charges is strongly associated with the geometry of a metallic nanostructure, incident polarization state of light and incident wavelength. Mechanism of induced charge redistribution directly functionalizes the main operation of a metallic nanostructure. In addition, surface current distribution is mainly followed by induced charge redistribution and it is directly associated with near- and far-field radiation pattern. Basically, induced charges of a metallic nanorod are redistributed featuring dipole moment when illuminated by the parallel polarization state of light to the axis of a metallic nanorod. Various novel metallic nanostructures feature their unique induced charge distribution models. On the other hand, these well-known metallic nanostructures have a drawback such as strongly polarization-dependence. Control of induced charge redistribution enables the issue of polarization-dependence to resolve. Therefore, new type of a metallic nanostructure can be constructed on the basis of induced charge redistribution. It also provides the opportunity to develop versatile nanophotonic components.

In attempt to unravel a couple of obstacles in a subwavelength scale, many researchers have been focused on achieving light concentration and confinement by tailoring metallic structures. Traditionally, the dielectric lenses and resonators have been exploited to concentrate light and produce high local field-intensity. These objects can offer a useful way to manipulate and enhance the light. However, dielectric lens cannot focus the light to tiny spots less than approximately half a wavelength of light and dielectric resonators have the limitation of electromagnetic mode volumes up to $(\lambda/2)^3$, where λ is the wavelength of light inside the dielectric medium. On the other hand, light concentrators and resonators adopted with metallic nanostructures are distinct and do not have limitations against the dielectric counterparts. Therefore, design and tailoring of metallic nanostructures for the certain purposes have been incessantly demanded. In addition, the use of metallic nanostructures is introduced to overcome the diffraction limits in a subwavelength scale. In a similar manner, the mechanism of induced charge redistribution plays the explicit role to define the optical properties. These characteristics

originate from the interaction between the electromagnetic field and free electron oscillation between dielectric and metal surface, known as surface plasmon. The explosion in research on plasmonics results from the developments of fabrication and measurement nanotechnology. This research has been flourishing, accompanying with breakthroughs in nanotechnology, such as the focused ion beam and the near-field scanning optical microscope.

1.3. Scope and organization

Plasmonic nanostructures have been recently considered as an attractive substitute in nanophotonic applications. In particular, metallic nanostructures are designed and utilized for the purpose of enhancing electromagnetic field intensity and confining radiating light fields. In this dissertation, metallic nanostructures are studied and exploited with the mechanism of induced charge redistribution mechanism.

This dissertation will be organized as follows. Chapter 1 briefly discusses the introduction of plasmonic nanostructures in optical regime and motivation of this dissertation. Mainly, the fundamental principles and theory of metallic nanostructures in optical regime are described in Chapter 2. Localized surface plasmon resonance is observed in the properly designed metallic nanostructure. Lightning rod effect is necessary to explain the phenomena of a metallic nanorod. In addition, the model of a localized nanocapacitor can be applied to the analysis of metallic nanostructures including a dielectric nanogap. In designing a metallic nanostructure for the purpose of field or radiation enhancement, it is required to hire effective wavelength scaling law. In addition, various induced charge redistributions are observed in well-known metallic nanostructures. Meanwhile, the analogy to electronics is adopted in optical region. Diverse types of microwave antenna have been developed and already commercialized in a wide range of cutting-edge technologies. These antenna types enable metallic nanostructures to be hired in optical regime to boost radiation intensity. Recently, optical

dipole antenna, optical monopole antenna and optical Yagi-Uda antenna have been theoretically and experimentally demonstrated [26]. Then, the last section of Chapter 2 depicts nano-scale transceiver system composed of coupled metallic nanorods and a metallic tip.

With the basis of fundamentals, I mainly proposed and demonstrated the novel type of a metallic nanostructure, plasmonic faced folded metallic nanorods, called FFR, in Chapter 3. Plasmonic faced folded metallic nanorods are composed of two folded metallic nanorods facing each other. The basic structure, single folded metallic nanorod possesses unique induced charge redistribution with regard to incident polarization states of light. This proposed structure is distinguished from coupled metallic nanorods or metallic nanoring due to *folding effect* shown in Section 3.1. Its characteristics via induced charge redistribution mechanisms are numerically analyzed and compared with reference structures in Section 3.2. Optimized processes and internal physics of FFR unit are identified in Section 3.3. Unique current paths appear in plasmonic faced folded metallic nanorods without regard to incident polarization state of light. In an attempt to experimentally verify the optical behavior of plasmonic faced folded metallic nanorods, three-dimensional holographic microscopy configuration is used. The intensity of the transmitted light through an FFR unit placed in an aperture is stronger than the intensity of the transmitted light through a bare aperture. Furthermore, the transmitted light passing through an FFR unit placed in an aperture is enhanced and concentrated in all planes presented in Section 3.4. Furthermore, the array of FFRs placed in a metallic nanoslit is numerically and experimentally examined.

Realistic issue of diffraction limit in a subwavelength regime can be dealt with the use of metallic nanostructures. Typically, a subwavelength metallic slit, called “nanoslit” possesses a crucial problem such as weak transmission due to diffraction limit. In Chapter 4, placing metallic nanostructures including the array of FFRs and metallic nanoislands inside a metallic nanoslit is introduced. I propose the embedded metallic nanoislands placed inside a metallic nanoslit for the purpose of overcoming weak

transmission. When metallic nanoislands are placed inside a metallic nanoslit, they can play a role to create tangible plasmonic modes in the proposed structure. These plasmonic modes allow the intensity of transmitted light to increase. The optical properties of the proposed structure are uniquely distinguished with the incident polarization state of light. In addition, the resonant wavelength of the proposed structure is tuned by the geometry and number of embedded metallic nanoislands. These observations are proved numerically and experimentally in Section 4.2.

Finally, concluding remarks and whole outlooks are addressed in Chapter 5.

Chapter 2

Fundamentals and charge redistribution mechanisms at plasmonic nanostructures

Surface plasmons (SP) are referred to as plasmons on the metal surface. Plasmons confined at metallic nanoparticles with a resonance are mentioned as localized surface plasmon (LSP). In this chapter, the fundamental physics of metallic nanoparticles or metallic nanostructures are concisely discussed. The use of metallic nanostructures to enhance optical characteristics attempts to change the light-matter interactions as an interface with the nanoscale. Distinct metallic nanostructures benefit from extreme light concentration and manipulation. These deliberate metallic nanostructures allow the antenna system to be launched in the visible and near infrared regime.

2.1. Fundamentals of plasmonic nanostructures

A metallic nanoparticle is considered as a basic structure of plasmonic nanostructure. After Mie's work in the early 20th century, the optical properties of metallic nanoparticles have been extensively studied. LSPR is essential to account for the resonance of metallic nanoparticle when the light impinges on metal surface. In addition, when metallic nanoparticles are periodically arrayed, the dimensions of dielectric nanogap act as a critical role to optimize the optical responses. Hence, the fundamental principles associated with plasmonic nanostructures are presented as follows.

2.1.1. Localized surface plasmon resonance

Aforementioned, surface plasmons can be considered as an interaction between matter and the electromagnetic field of the light. To analyze surface plasmons in a metal surface, the Maxwell equations with the appropriate boundary conditions are introduced. Localized surface plasmons are also associated with the same analysis in a localized metallic nanostructure. A metallic nanoparticle can be depicted as a lattice of ionic cores with conduction electrons moving almost freely inside the nanoparticle. When the particle is illuminated by incident light, the electromagnetic field of the light strives to force on these conduction electrons moving them towards the nanoparticle surface. When these electrons are confined inside the nanoparticle, negative charges will be accumulated on one side and positive charges in the other side. This is called an electric dipole. This dipole creates an electric field inside a metallic nanoparticle in opposition to the electromagnetic field of light that will force the electrons to go back to the equilibrium position. Hence, the electric dipole is larger with the increase of the electron displacement, leading to larger restoring force. It is analogous to a linear oscillator with a restoring force.

We can obtain the explicit form of electromagnetic field distribution using some assumptions when a particle interacts with electromagnetic field. First, we assume the particle size is much smaller than wavelength of light in the surrounding medium. In this

condition, the phase of the harmonically oscillating electromagnetic field is approximately constant over the particle volume. This is called quasi-static approximation. Second, we choose a simple geometry for analytical treatment: The particle is a homogeneous isotropic sphere of radius r_0, and surrounding material is a homogeneous, isotropic and non-absorbing medium. On the illumination of static electric fields, we solve Laplace equation for the potential, $\nabla^2 V = 0$. Due to the azimuthal symmetry of the problem and requirement that the potentials remain finite at the center of the particle, the solutions of this Laplace equation for potentials inside and outside the particle can be written as:

$$\begin{aligned} V_{\text{in}}(r,\theta) &= \sum_{l=0}^{\infty} A_l r^l \, \mathrm{P}_l(\cos\theta), \\ V_{\text{out}}(r,\theta) &= \sum_{l=0}^{\infty} \left[\mathrm{B}_l r^l + \mathrm{C}_l r^{-(l+1)} \right] \mathrm{P}_l(\cos\theta), \end{aligned} \tag{1}$$

where $\mathrm{P}_l(\cos\theta)$ is the Legendre polynomial of order l, and θ is the angle between the position vector $\mathbf{r}$ and the electric field $\vec{\mathbf{E}}$. The coefficients A_l, B_l, C_l can be determined using boundary conditions: as r approaches infinity, the potential approaches $-|\vec{\mathbf{E}}|\, r\cos\theta$, the tangential components of electric fields are equal at $r = r_0$, and normal components of electric flux density are equal at $r = r_0$. The solutions are:

$$\begin{aligned} V_{\text{in}} &= -\frac{3\varepsilon_{\text{d}}}{\varepsilon_m(\omega) + 2\varepsilon_{\text{d}}} \left|\vec{\mathbf{E}}\right| r\cos\theta, \\ V_{\text{out}} &= -\left|\vec{\mathbf{E}}\right| r\cos\theta + \frac{\varepsilon_m(\omega) - \varepsilon_{\text{d}}}{\varepsilon_m(\omega) + 2\varepsilon_{\text{d}}} \left|\vec{\mathbf{E}}\right| r_0^3 \frac{\cos\theta}{r^2}. \end{aligned} \tag{2}$$

Here, $\varepsilon_{\text{m}}(\omega)$ and ε_{d} are electric permittivity of metal and surrounding dielectric layer, respectively.

We can interpret V_{out} physically: V_{out} is the superposition of the applied field and a dipole induced by this field. Therefore, we introduce the dipole moment $\vec{\mathbf{p}}$ as:

$$\vec{\mathbf{p}} = 4\pi\varepsilon_0\varepsilon_{\text{d}} r_0^3 \frac{\varepsilon_m(\omega) - \varepsilon_{\text{d}}}{\varepsilon_m(\omega) + 2\varepsilon_{\text{d}}} \vec{\mathbf{E}}. \tag{3}$$

If we introduce polarizability α via $\vec{\mathbf{p}} = \varepsilon_0\varepsilon_{\text{d}}\alpha\vec{\mathbf{E}}$, we can express α as:

$$\alpha = 4\pi r_0^3 \frac{\varepsilon_m(\omega) - \varepsilon_{\text{d}}}{\varepsilon_m(\omega) + 2\varepsilon_{\text{d}}}. \tag{4}$$

We can expand Eq. (4) in case of arbitrary shaped particle as [27]:

$$\alpha = (1+\kappa)\varepsilon\Omega\frac{\varepsilon_m(\omega)-\varepsilon_d}{\varepsilon_m(\omega)+\kappa\varepsilon_d}, \quad (5)$$

where Ω is the volume of the particle. As can be seen, the dipolar polarizability α could be maximized at the condition of $\mathrm{Re}(\varepsilon_m(\omega)) = -\kappa\varepsilon_d$, which is denoted by the resonance condition of LSPR assuming $\mathrm{Im}(\varepsilon_m(\omega))$ is relatively small and constant value with the variation of frequency. κ is a shape factor that embodies geometrical polarizability of the surface that indicates the electron oscillations. The shape factor of a small nanostructure plays a critical role to increase dipolar polarizability for enhancing LSPR strength. This variable can be straightforwardly expressed by aspect ratio [28].

2.1.2 Lightning rod effect

Gersten and Nitzan discussed the electromagnetic model in such a metal ellipsoid as for the enhancement [29]. Three sources of enhancement were denoted by the image dipole effect, the increase in local field caused by "lightning rod effect", and the resonant particle plasmon effect. Among them, "lightning rod effect" comes from the major two factors. The first factor is considered as dipolar fields of the particle plasmon resonance and the second factor is a purely geometric factor which is called "lightning rod factor". If the major a and minor b axis dimensions of an ellipsoid are a and $b << \lambda$, the electrostatic approximation can be used. From the point dipole approximation, the resonant enhancement increases as metallic particles are made more needlelike. To describe the depolarizability in metallic nanoparticle, the depolarization factor A is given by

$$A \sim \left(\frac{b}{a}\right)^2 \ln\left(\frac{a}{b}\right) \quad (6)$$

for highly prolate ellipsoids. The lightning rod induces strong electric field near the metallic tip as charge tends to accumulate at a sharper edge. Its definition is strictly related to the concentration of the fields at the metallic edges and tips of particle shape. This effect results from the dipolar fields of a particle, which is concentrated near their edges or tips. Due to the lightning rod concentration of the fields, the magnitude of the

enhancement is not strongly related to the optical properties of the surface but the particle dipole moment.

2.1.3 Modeling of localized nanocapacitor

When the metallic nanostructure is excited by light, enhanced electric fields in a vicinity of metallic edges are typically accompanied by a surface charge oscillation. In such a metallic bow-tie antenna or nanoparticle dimer, plasmonic enhancement of electric field increases in a gap nestled between metallic edges. This gap structure is supposed to be the "capacitance" of the whole structure and subsequently induces the electric field. Although the conventional concept of static capacitance fails to apply, the capability of controlling enhancement through capacitance would play a key role in nanoscale optical devices. To predict the strong enhancement of electric fields near subwavelength metallic structures, "λ-zone" capacitance for plasmonic systems is introduced [30]. The λ-zone capacitance, defined as a static local capacitance with confined region of wavelength dimension, is considered for a metallic slit with a narrow gap or a metallic tip near a metallic surface or two metallic rods forming a gap. When an electromagnetic wave impinges upon a metal, current is induced, resulting from the high conductivity of metal. The current density occupies mostly at the surface within the skin-depth region and can be replaced by an effective surface current.

2.1.4 Effective wavelength scaling in optical antenna

Traditionally, microwave antenna design makes use of geometry with characteristic length L that is directly related to the wavelength λ of outgoing radiation. For example, an ideal half-wave dipole antenna is scaled as a thin rod of length $L=\frac{1}{2}\lambda$. On the other hand, the simple wavelength scaling breaks down because incident radiation is no longer perfectly reflected from the metal surface at optical frequencies. Radiation penetrates into

the metal and creates oscillations of the free-electron gas. Thus, an antenna hardly responds to the external longer wavelength instead, shorter wavelength at optical frequencies [30]. In optical regime, effective wavelength λ_{eff} depends on the metal material properties and physical variables. In addition, due to the effect of localized surface plasmons in a metal at optical frequency, surface plasmon wavelength λ_{spp} should be considered [31] and is expressed as:

$$\lambda_{spp} = \lambda \sqrt{\frac{\varepsilon_m + \varepsilon_d}{\varepsilon_m \varepsilon_d}} \tag{7}$$

The antenna length has to be adjusted in relation with the wavelength and angle or polarization of incidence.

2.2. Induced charge redistribution at various metallic nanostructures

In designing a plasmonic nanostructure in optical regime, much effort has been devoted for extreme light concentration and manipulation. Fundamentally, a metallic nanoparticle excited by incident light with the appropriate wavelength can give rise to localized surface plasmon resonance. However, it is too weak intensity to apply for the nanophotonic applications. Hence, the design of a metallic nanostructure should be required for additional field enhancement. In this section, several methodologies for additional field enhancement are explicated.

2.2.1 The use of inter-coupling between metallic nanoparticels

When two metallic nanoparticles are close to each other, the inter-coupling between two nanoparticles can be achieved, arisen from localized capacitive coupling at the air nano-

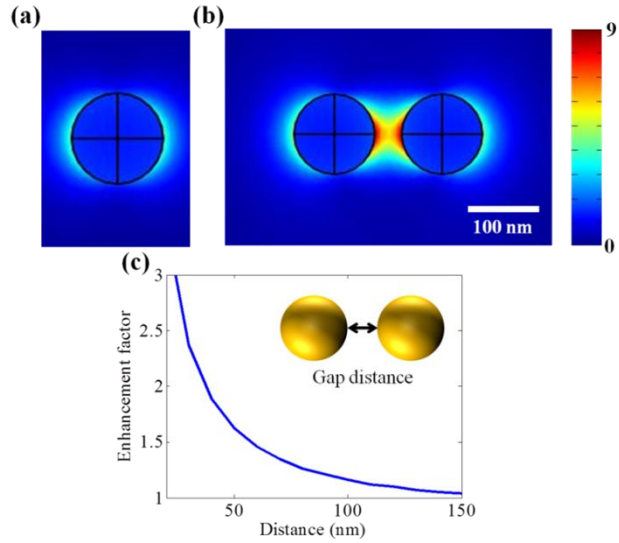

Figure 2.2.1 Electric field distributions (V/m) at (a) a single Au nanoparticle and (b) Au nanoparticle dimer when the incident wavelength of light is 633 nm and the magnitude of incident field is 1 (V/m). The diameter of Au nanoparticle is 100 nm. These calculations are based on finite element method; (c) Field enhancement factor of Au nanoparticle dimer with respect to the single nanoparticle. In all simulations in this figure, the radius of each nanoparticle is 50 nm.

gap surrounded by nanoparticles as shown in Fig. 2.2.1(a)-(b). Such an enhancement originates from the charge induction between two nanoparticles, which interact stronger as they get closer to each other. This relation between the field enhancement factor of nanoparticle dimer and gap distance is clearly shown in Fig. 2.2.1(c). A metallic nanoparticle array has been extended from this phenomenon. The optical properties of a metallic nanoparticle array are mainly determined by the periodicity and spacing distance [31].

2.2.2 Plasmonic nanostructures using sharp edges

Another promising method for plasmonic enhancement in a metallic nanostructure is using either multi-polar resonance or metallic sharp edges with regard to induced charge redistribution. Adopting a sub-10 nm sharp edge or tip, extremely high field intensity can be achieved at the metallic nanocrescent. Localized and confined electromagnetic field

enhancement, which is mentioned as “hot spot”, is attracting much attention. As shown in Fig. 2.2.2, localized field intensity is much larger at the edges of a nanocrescent. The shape and dimension of a metallic nanocrescent should be precisely designed to manipulate induced charge distribution. Also, one of the major physical variables for designing a metallic nanocrescent is the width of a nanocrescent since it is strongly relevant to the structural polarizability. Figs. 2.2.2(a)-(b) present the field distribution near the nanocrescent with the width of 50 nm, whereas Figs. 2.2.2(c)-(d) show that of 100 nm. In comparisons with two structures, it can be shown that the local field intensity is slightly larger at the 50 nm width nanocrescent. This can be accounted for the relationship between shape factor and aspect ratio, which indicates that more needle-like

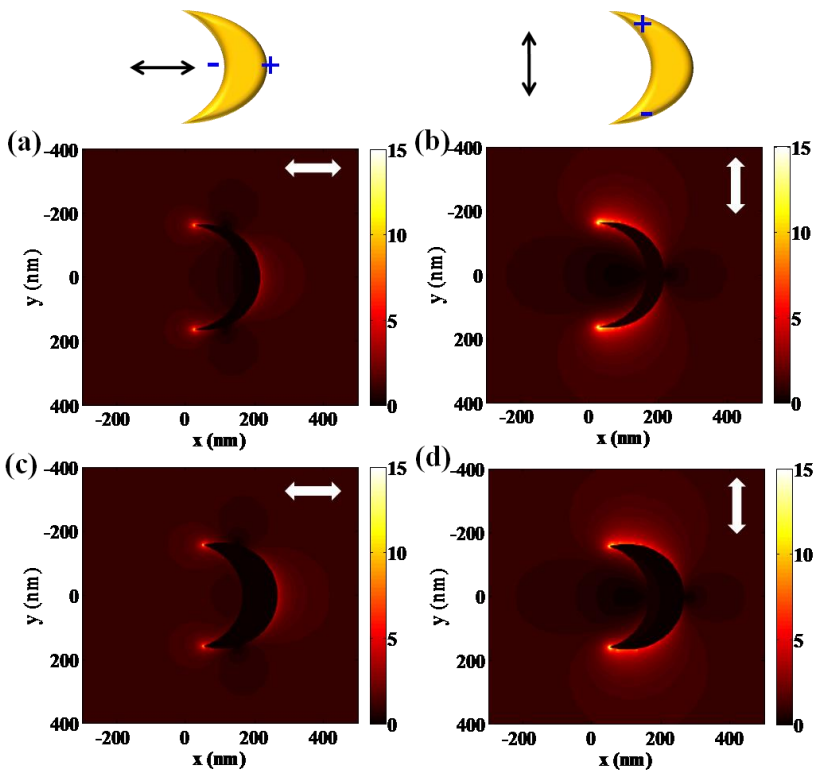

Figure 2.2.2. Intensity distributions (arbitrary unit) of a metallic nanocrescent with respect to the width of nanocrescent and incident polarization state of light: (a) 50 nm wide and horizontally polarized light, (b) 50 nm wide and vertically polarized light, (c) 100 nm wide and horizontally polarized light, (d) 100 nm wide and vertically polarized light.

structure can strongly enhance the field. Moreover, the degree of enhancement at a metallic nanocrescent strongly relies on the polarization state of light. When illuminated by vertically-polarized light, higher field intensity can be observed as compared with the incidence of horizontally polarized light. This phenomenon can result from the difference of accumulated electrons at the sharp edges in a nanocrescent. Horizonatlly-polarized light equally separates the electrons to the both ends of nanocrescent, whereas vertically-polarized light enables electrons to totally move to sharp edges of a nanoscrescent, which leads to higher field intensity. Furthermore, some of structures can be explained by the composition of both multipolar resonance and inter-coupling of nanoparticles. For example, double nanocrescents facing each other are a representative case [32]. As illustrated in Fig. 2.2.3, the intensity distributions of double nanocrescents are similar to the optical responses of a single nanocrescent and sensitively respond to incident polarization of light. However, they can generate much higher field intensity. Enhanced field intensity calculated at double nanocrescents is approximately two times larger than that of single nanocrescent for the vertically polarized case, and even higher for the horizontally-polarized case. This supports that localized capacitive inter-coupling nestled

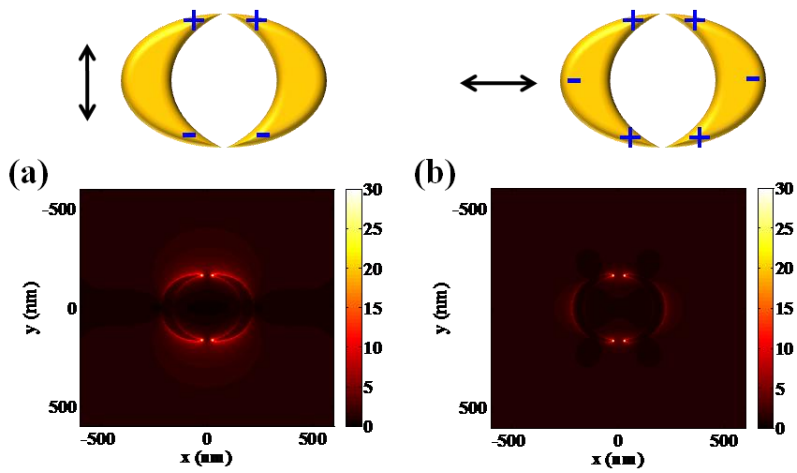

Figure 2.2.3. Intensity distributions (arbitrary unit) of metallic double nanocrescents with respect to incident polarization state of light: (a) vertically-polarized light and (b) horizontally-polarized light. The width of a nanocrescent is fixed to 50 nm.

at nanogaps is attributed to the enhancement of field intensity in a single nanocrescent structure. This inter-coupling effect is more effectively observed with horizontally-polarized light, which can be described by the attraction between the oppositely induced charges at the end of nanocrescents.

The other distinct nanostructure for additional field enhacement is the metallic nano-star. Hao *et al.* addressed the metallic nanostar structure explicitly separating local excitations [33]. A nanostar is composed of a central core from which a number of protruding tips extend. They typically distinguish with an LSPR of the core and multiple LSPRs corresponding to the tips and core-tip interactions. The latter is polarization dependent and accompanied by large local electric field enhancements at the sharp ends of the tips. It can be explained by the hybridization of plasmons associated with the core and individual tips of the metallic nanoparticle. The electric near-field enhancement arisen from tip plasmon modes is given by the size of the core, as a result of hybridization of tip

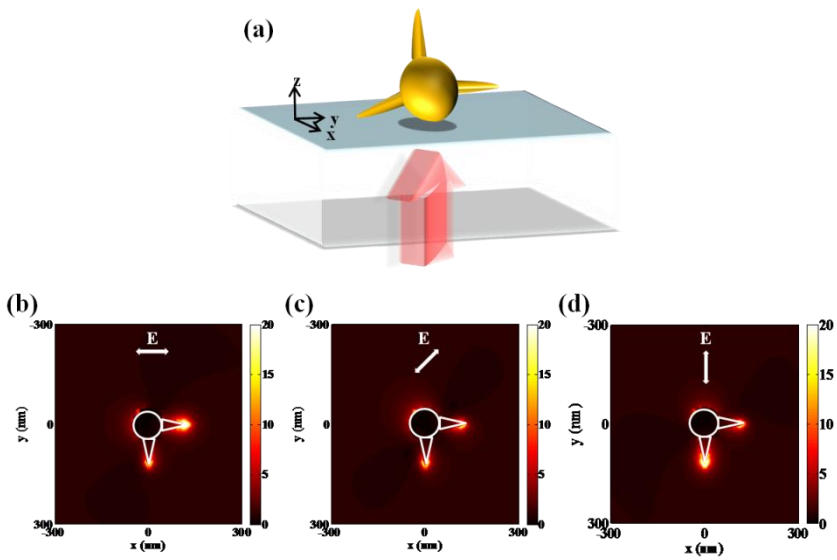

Figure 2.2.4. (a) Schematic of a simplified metallic nanostar placed onto a glass substrate. Electric field distributions at a distance of 10 nm above a nanostar when illuminated by (b) horizontally-polarized light; (c) 45°-polarized light; and (d) vertically-polarized light.

and core modes. Individual plasmonic hot spots in a single gold nanostar can be selectively produced at the tips with respect to the wavelength and polarization of incident light [34]. To investigate the optical response of a metallic nanostar in visible range, electric field distributions from a simplified nanostar structure are numerically calculated in Fig.2.2.4. Unique properties of three-dimensional structure can generate specific field pattern in response to the variation of the polarization state of light. Resonant frequency or wavelength is based on the length scale of individual tips assuming that core dimension is fixed.

2.3. The analogy with microwave antenna in optical regime

Fumbling with metallic nanostructures, plasmonic antenna has been introduced in analogy with microwave antenna. A metallic nanorod has been proposed as an optical dipole antenna. Hence, the metallic nanorod and coupled metallic nanorods as a plasmonic antenna are mainly investigated with regard to the scattering properties and field enhancement arisen from LSPR and lightning rod effect. The antenna properties depend on those of the receiver-transmitter, and it becomes evident that these must be regarded as a coupled system. When coupled nanorods are illuminated by the incident light with the proper wavelength, electromagnetic field enhancement can be obtained from the static capacitive coupling at the nanogap across the coupled nanorods. Moreover, stronger field enhancement at the edges of metallic nanorods can be observed because the electric charges in the metal accumulate at edges and be polarized. Figure 2.3.1 illustrates the nano-scale antenna system composed of coupled nanorods and a metallic tip in visible range. In a microwave range, antenna system consists of transmitter, receiver and radiation space. In the proposed system here, coupled metallic nanorods are assumed to be a transmitter and a metallic tip is also assumed to be a receiver. However, different from the antenna system in a microwave range, radiation space in this transceiver system is ranged in a few nanometers. These nano-scale antennas can be utilized for the nano-optic applications including optical data storage, bio-sensing and field spectroscopy.

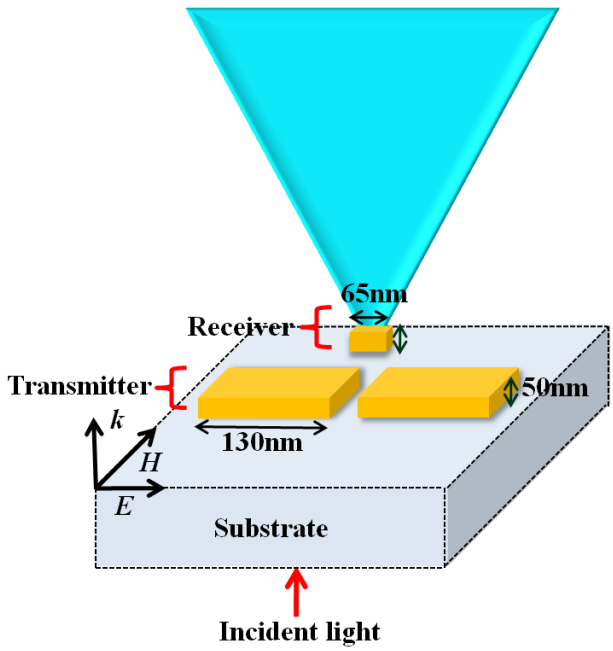

Figure 2.3.1 Schematic of nano-scale transceiver antenna system composed of coupled metallic nanorods and a metallic tip in visible range.

In particular, nano-scale antenna systems are recently demanded on the application of SERS (Surface-Enhanced Raman Scattering) and SPR bio-sensing in visible and near-infrared range. In a proposed geometry, coupled metallic nanorods consist of 130 nm two gold nanorods including a 20 nm air nanogap. A 65 nm gold nanorod is employed as a metallic tip. Spacing between coupled metallic nanorods and a metallic tip is enlarged from 20 nm to 30 nm. Numerical analysis is performed with FDTD (Finite-Difference Time-Domain) method to examine the spectrum and electromagnetic field distributions. Although the optical antenna systems have poor antenna reception, this structure shows that field coupling from coupled-rods to a metallic tip occurrs at nano-scale spacing distance. In an attempt to investigate the spectrum in response to the variation of spacing distance between the transmitter and receiver, each spectrum is calculated as shown in Fig. 2.3.2. The resonance regime is observed between 300 THz and 400 THz in the spectrum of coupled metallic nanorods (Fig. 2.3.2(a)). The spectrum of coupled metallic

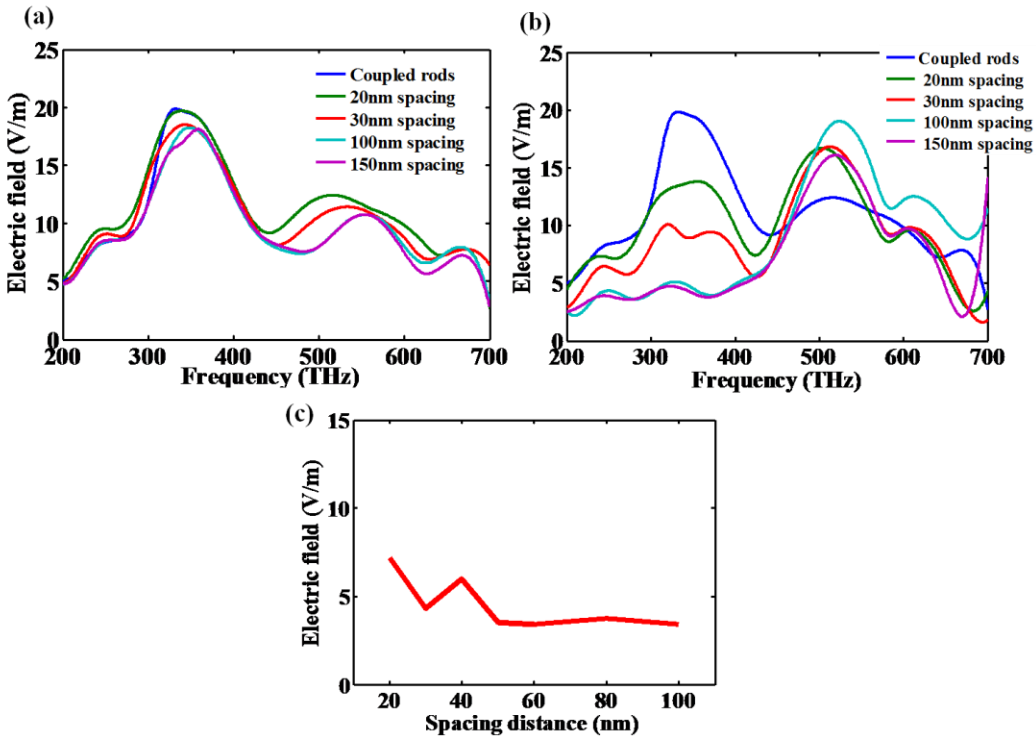

Figure 2.3.2. (a) Spectra according to the spacing distance on coupled metallic nanorods as a transmitter, (b) spectra according to the spacing distance on a metallic nanotip as a receiver, and (c) the degree of electric field magnitude according to the spacing distance. These calculations are performed with the incidence of horizontally-polarized light. The magnitude of incident electric field is 1 (V/m).

nanorods is independent of the spacing distance from a metallic tip. However, the spectrum of a metallic tip is different from the spectrum of coupled metallic nanorods. The magnitude of electric field is saturated over at 50 nm spacing distance. Figure 2.3.3 presents the electric field intensity distributions in the radiation space between coupled metallic nanorods (i.e., transmitter) and a metallic nano-tip (i.e., receiver). Even though the intensity at a metallic nano-tip gets weaker as the spacing distance between transceiver increases, it allows the nano-scale transceiver system to couple each other. According to these numerical calculations, nano-scale metallic transceiver system would be realized with regard to incident wavelength, polarization state of light, and target applications.

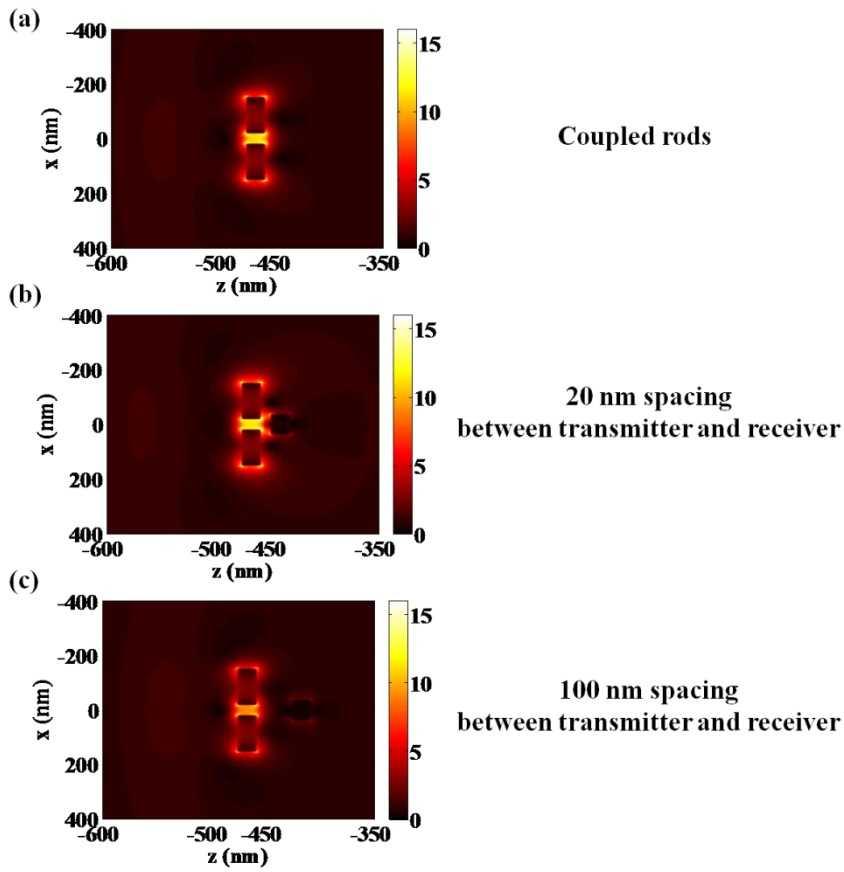

Figure 2.3.3. Intensity distributions of (a) coupled metallic nanorods, (b) 20 nm spacing between transmitter and receiver, and (c) 100 nm spacing between transmitter and receiver.

Chapter 3

Plasmonic faced folded metallic nanorods as a compact light concentrator

3.1. Folded metallic nanorod and plasmonic faced folded metallic nanorods in visible range

The re-radiation of plasmonically concentrated and enhanced light into free space has attracted significant research interests. The most well-known examples are extraordinary optical transmission (EOT) and beaming phenomena [35, 36]. The re-radiation accompanying field enhancement or concentration by a properly-designed metallic nanostructure can be effectively described by using the well-known terminology of antenna. In a view of plasmonic antennas, the manipulation of light emission from metallic structures is of great concerns to ensure the functionality as well as light concentration. To manipulate the radiation properties of light in plasmonic nanostructures, the shape, type of metals and the wavelength of incident light should be appropriately chosen for SPs to be efficiently excited in a desired way. For example, the radiation from a metallic nano-rod shows a far-field pattern analogous to that of a dipole antenna in radio frequencies [37]. By controlling shape, dimension, and spatial arrangement of such nano-rods, radiation characteristics can be manipulated. Therefore, properly-designed metallic nanostructures can offer a convenient way to concentrate light waves. On the other hand, they have still some of drawbacks. For example, coupled metallic nanorods when illuminated by incident horizontally-polarized light in the axis

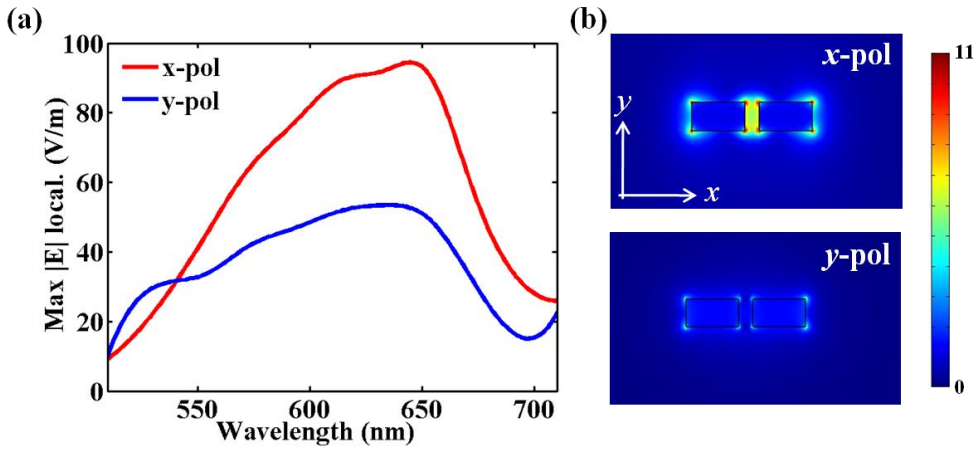

Figure 3.1.1. Optical properties of coupled metallic-nanorods (a) spectrum with respect to the *x*-polarized and *y*-polarized light (b) electric field distribution at z = 120 nm with respect to the *x*-polarized and *y*-polarized light, respectively.

have been experimentally demonstrated, presenting highly localized field strength at a metallic nanogap. But, on the incidence of vertically-polarized light, highly localized field intensity cannot be observed at the coupled metallic nanorods. It means that the optical performance of coupled metallic nano-rods is strongly polarization-sensitive. Another outstanding plasmonic structure, plasmonic bow-tie antenna, is taken into account for the field enhancement and concentration of light as well. This structure is also regarded as polarization-sensitive. Although these recently reported structures produce significantly strong re-radiation intensity in a free space when incident polarization direction is along their major axis, these structures suffer from the critical weakness including the property of polarization-sensitive. Here, I propose the attractive plasmonic nanostructure showing both remarkable near- and far-field enhancement and polarization-insensitivity. In addition, analogy with microwave antenna allows it to be applied to optical regime as mentioned above. One of the best antennas in microwave regime is folded dipole antenna. It is defined as a dipole antenna with the ends folded back around and connected to each other, forming a loop as shown in Fig. 3.1.2. The input impedance of the folded dipole is four times larger than that of half-wave dipole antenna [38].

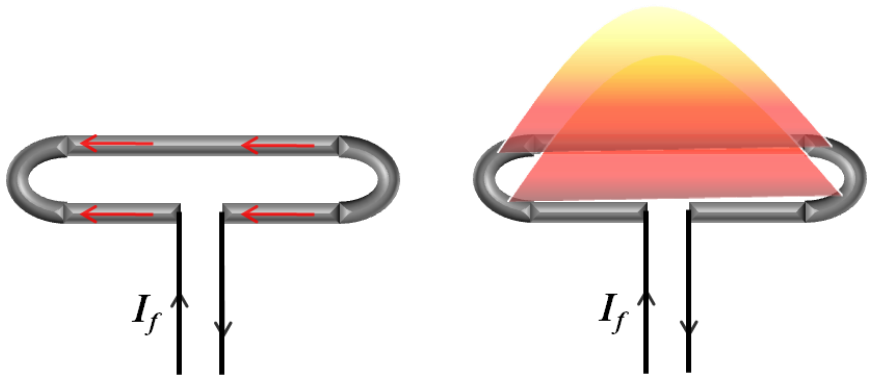

Figure 3.1.2. Current distribution and radiation profile on folded dipole antenna in a microwave regime.

Based on this approach, a folded metallic nanorod is addressed. As a prototype, L shaped or C shaped metallic nanoapertures present folded region in the counterpart of folded metallic nanorod, acting as the deposit of accumulated charge by induced electric field. When illuminated by *x*-polarized light in a single folded metallic nanorod, localized field spots are observed in two folded regions inside a single folded metallic nanorod. This phenomenon can be analogous to the optical response of complementary nanoaperture, caused by accumulated charges. In addition, distinct field distributions are observed with regard to the incident polarization state of light in a single metallic nanorod. It originates from the *folding effect* in a single folded metallic rod. To boost the localized field intensity, two single folded metallic rods face each other. It is called plasmonic faced folded metallic nanorods (call FFR) here. It is numerically investigated further and experimentally demonstrated for the use of the FFR unit as a field concentrator in the far-field region. Plasmonic faced folded metallic nanorods are proposed as one of tailored metallic nanostructures and a compact light concentrator here. It is composed of two folded metallic nanorods placed facing each other. We performed the numerical analysis of the FFR unit using the three-dimensional finite difference time domain (FDTD) method [39], using the Palik parameters for the permittivity of Au [40], and assuming normal plane waves (wavelength = 633 nm) incident uniformly from the rear side of the SiO_2 substrate (having a refractive index of 1.46 at 633 nm). We extracted the structural

parameters shown in Fig. 3.1.4(a) based on the assumption that the more enhanced the local fields of the FFR unit are, the better far-field characteristics we can obtain.

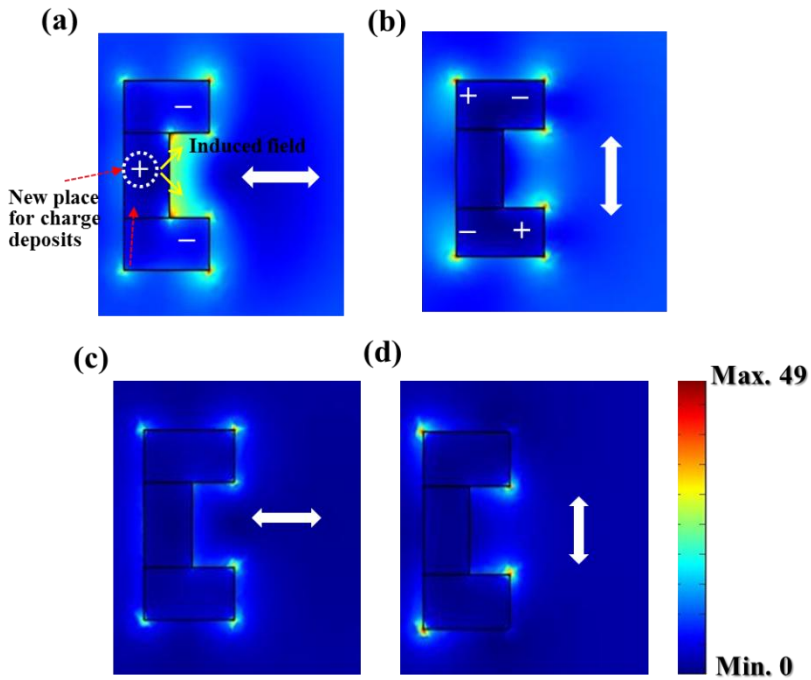

Figure 3.1.3. Electric field distribution of a single folded metallic nanorod when illuminated by (a) *x*-polarized light and (b) *y*-polarized light at the middle depth (z = 65 nm). (c) and (d) are electric field distribution when illuminated by *x*-polarized light and *y*-polarized light at the top surface (z = 130 nm), respectively.

This indicates that we optimized the FFR structure in such a way that its local fields via the surface plasmons are maximized. For this purpose, the design rules given in [41] with the Barbinet principle [42] are taken into consideration. At first, a single folded rod in free space is started. The incident wavelength sets to be 633 nm. Initially, the length of horizontal and vertical parts of the single folded rod were set to be approximately quarter and half of the surface plasmon wavelength ($\lambda_{SPP} \sim 600nm$), respectively. By iterative numerical calculations, the optimum values of the geometrical parameters are derived except for the gap between two single folded rods.

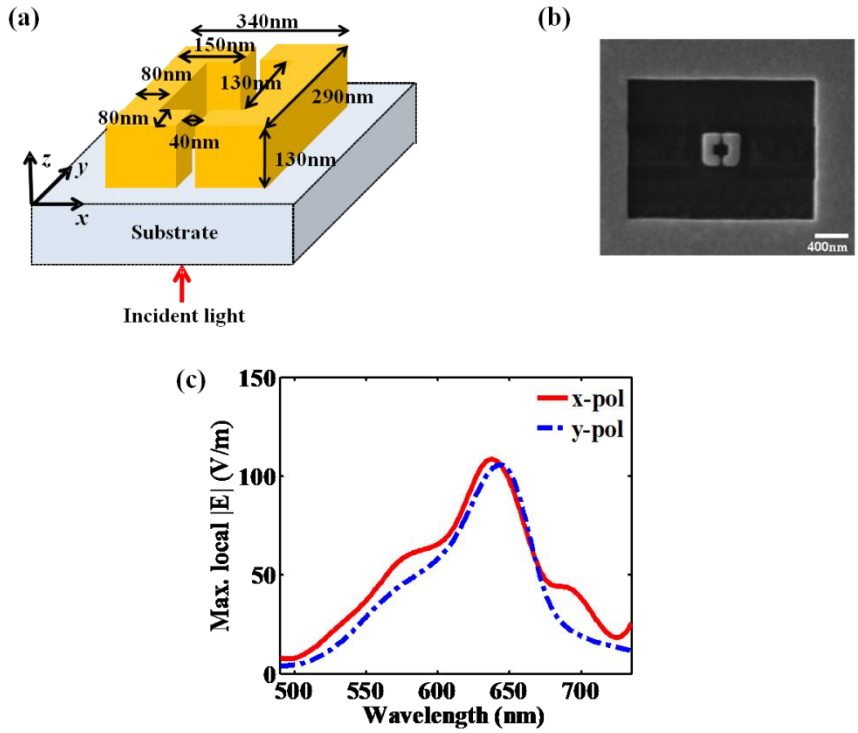

Figure 3.1.4. (a) Schematic of faced folded metallic nanorods, (b) exemplary sample of fabricated FFR unit placed in a bare aperture (2 μm x 2μm) and (c) spectra of FFR unit in free space according to the incident polarization state of light. The magnitude of incident electric field is 1 (V/m). Maximum values of local electric field upon the upper surface of an FFR unit are plotted.

To determine an appropriate gap size, we have to consider the fabrication capability of our FIB system. Numerically we found that the local fields do not grow or increase significantly if the gap size becomes smaller than 40 nm, which is actually comparable to the minimum object size our FIB system can make with high reliability. Therefore, we determined the gap size to be 40 nm. The exemplary fabricated SEM picture of FFR unit placed in bare aperture is shown in Fig. 3.1.4(b). Since it is hard to fabricate FFR unit on the glass substrate, FFR unit is located in the center of a square aperture, keeping the distance between FFR and a surrounding metallic wall to avoid any coupling between them. Figure 3.1.4(c) shows the plot of maximum local fields on the top surface of the FFR unit.

It provides that optimal resonant wavelength is approximately located between 630 nm and 640 nm regardless of incident polarization state of light. It confirms that FFR unit is designed to operate optimally near the visible wavelength of 633 nm. In addition, it is obvious that optical responses of the FFR unit will be independent of the polarization states of the incident light due to the uniqueness of FFR geometry. In Fig. 3.1.5(a), the degree of field enhancement is approximately similar regardless of incident polarization state of light. It can be taken account of polarization-insensitive structure. Due to the geometrical symmetry, electromagnetic field enhancement arisen from FFR unit can be obtained from both *x* component and *y* component of electric fields, respectively in Fig. 3.1.5(b). As shown in Fig. 3.1.5(c), capacitive coupling nested in 40 nm air nanogap contributes to increase of the strength in the *x*-component of electric field. Meanwhile, hot spots are observed in sharp edges located at an FFR unit in the *y*-component of electric field in Fig. 3.1.5(d).

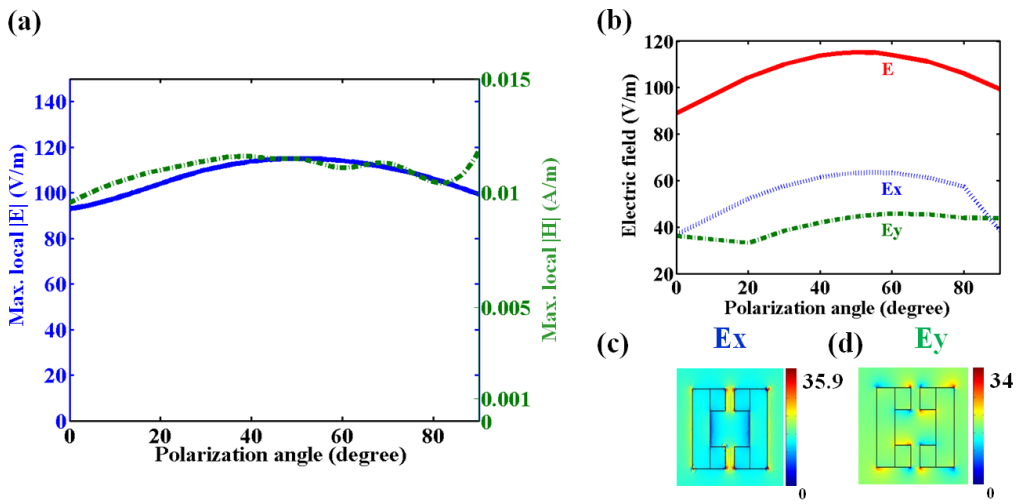

Figure 3.1.5. (a) Effects on the incident polarization angle of light and (b) the degree of enhancement in *x*- and *y*- components of electric field in comparison with total electric field, and field distribution of (c) *x*- and (d) *y*- components of electric field, respectively.

3.2. Induced charge redistribution mechanisms of FFR unit with regard to the polarization state of light

The optical properties of FFR unit can be distinguished from the incident polarization state of light, as mentioned above. Let us first consider the case when the illuminating light is polarized along the horizontal or *x*-direction. In Figs. 3.2.1 (a)-(c), the intensity and the magnitude/direction of the electric fields inside the FFR unit (z = 65 nm) with the current flows at its top surface are plotted. From the results, we can easily see that the most dominant fields in the FFR unit appear across two narrow (40 nm) gaps along the *x*-direction. They are due to the so-called capacitive coupling effect, i.e., created by the accumulated charges near the sharp edges of the rods (charges by the depolarization of surface charges [43]), whose oscillations can enhance the far-field radiation significantly [44]. Moreover, the interface between these radiation from upper and lower gaps can increase further the light intensity in the far-field region just as a folded dipole antenna in RF regime provides a four-fold-enhanced radiation over its dipole version. These indicate that the parts of the folded rods parallel to the polarization direction of the illuminating light play major roles in the overall response of the FFR unit. For the comparison, the responses of double (upper and lower) coupled-rods, which are placed only along the *x* direction in Figs. 3.2.1(d)-(f) are shown. It clearly identifies that when the incident light is *x*-polarized, the optical resonance of the FFR unit can be approximated into that of double coupled-rods. However, there is more than this in the FFR unit. The contributions of the vertical (placed perpendicular to the polarization direction) part of the folded rod are investigated as follows. This vertical part acts as a bridge between upper and lower rods, providing a new path for the charge exchange. Due to this path, semi-circular current flows are induced as shown in Fig.3.2.1(c). Basically, far-field radiation pattern is determined by surface current distribution according to antenna theory.

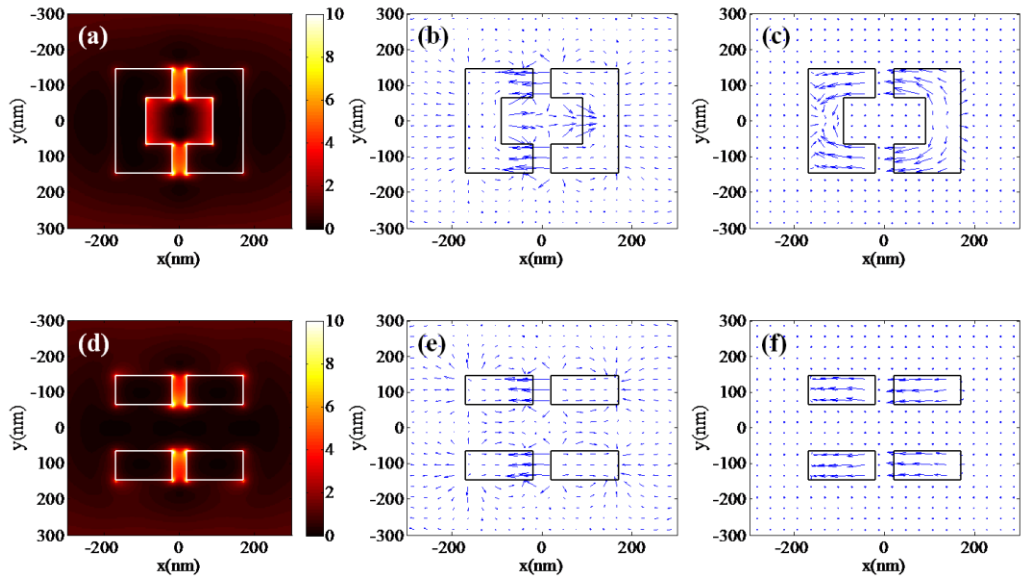

Figure 3.2.1. (a) Intensity, (b) magnitude/direction of the electric fields inside the FFR unit (z = 65 nm) at a specific phase at which the capacitive electric fields across two narrow gaps are maximized, and (c) distribution of the current flows at the top surface of the FFR unit at π / 5 after the phase used in (b). Note that it takes about π / 5 for the electric field shown in (b) to reach the top surface. (d) Electric field intensity of double (upper and lower) coupled-rods. In case of horizontally-polarized illumination, the optical response of the FFR unit is very similar to this. (e) magnitude/direction of the electric fields inside double (upper and lower) coupled-rods (z = 65 nm) at a specific phase at which the capacitive electric field across two narrow gaps are maximized, and (f) distribution of the current flows at the top surface of double coupled-rods. From (a) to (e), the illuminating light is x-polarized.

Hence, semi-circular current flowing in the FFR unit can contribute to concentrating the transmitted light. In Fig. 3.2.1, relatively strong fields near the vertical parts of the folded rods are found, resulting from this *folding effect*, not visible in the coupled-rod structure. It is noted that these fields should be distinguished from those originated from the capacitive coupling via an interior space [180 nm (x) x 130 nm (y), which can be considered as additional gaps for each direction], because the electric fields near the center of the interior space almost vanish. Therefore, it can be concluded that when the illuminating light is polarized horizontally, the FFR unit can be approximated into *horizontal dual dipoles* formed by the capacitive coupling effect via the narrow nanogaps

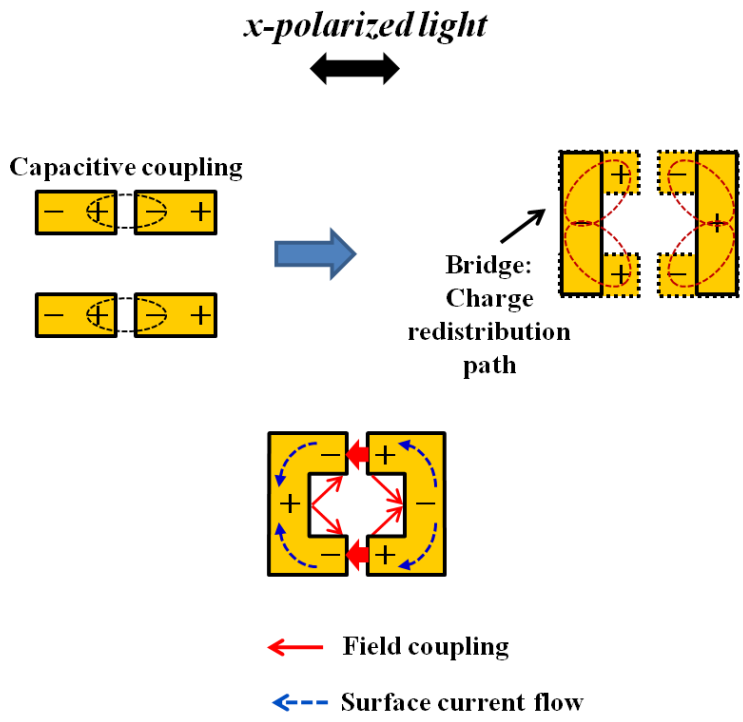

Figure 3.2.2. Charge redistribution model when FFR unit is illuminated by *x*-polarized light. The vertical part of the folded rod is like a bridge between upper and lower rods and becomes a new path for the charge exchange. Semi-circular current flows can be induced due to these vertical parts. However, it is noted that dual dipoles induced via the capacitive coupling play key roles and the effects of charge exchange or redistribution through the vertical parts are rather weak.

with semi-circular current flows induced via the vertical parts of the folded rods as illustrated in Fig. 3.2.2, and its overall radiation pattern in the far-field region is determined by these semi-circular current flows.

Let us turn our attention to the vertically-polarized illuminating case. Calculated electric field distribution inside the FFR unit (z = 65 nm) and the current flows at its top surface are presented in Figs. 3.2.3. For the comparison, the responses (field intensity) of two vertical rods of the same length as FFR unit in Figs. 3.2.3 (d)-(f) are presented [45]. These rods, which are placed only along the y direction, do not show any resonance feature, which indicates that the strong field inside of the FFR unit results mostly from the horizontal parts of the folded rods (It should be mentioned that this does not mean

that the vertical parts do not contribute to the resonance since it is quite evident that the motion of electrons along the vertical parts of the folded rods is excited directly by the vertically-polarized illumination and the resultant depolarization of surface charges are one of key factors for the resonance.) Their effects are shown schematically in Fig. 3.2.4: upper and lower horizontal parts provide short paths for charge deposits which in turn induce capacitive coupling between them. Since there are two single folded rods in the FFR unit which are placed very close (~ 40 nm) to each other and have mirror-symmetric charge distributions, their respective capacitive couplings interfere constructively in the interior into *vertical dual dipoles* formed through semi-circular current flows.

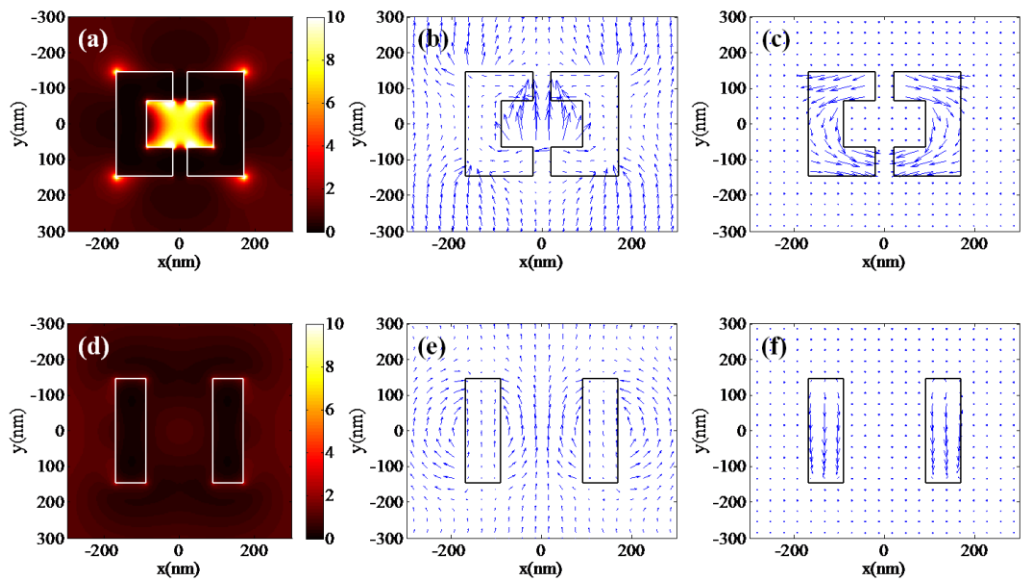

Figure 3.2.3. (a)-(c) The same as Fig. 3.2.1 when the illuminating light is *y*-polarized, in which case the optical response of the FFR unit is completely different from that of two vertical rods whose electric field intensity is plotted in (d). Here the phase taken in (b) is when the electric fields in the interior of the FFR unit are maximized. (e) magnitude/direction of the electric fields inside two vertical rods (z = 65 nm), and (f) distribution of the current flows at the top surface of two vertical rods. From (a) to (e), the illuminating light is *y*-polarized.

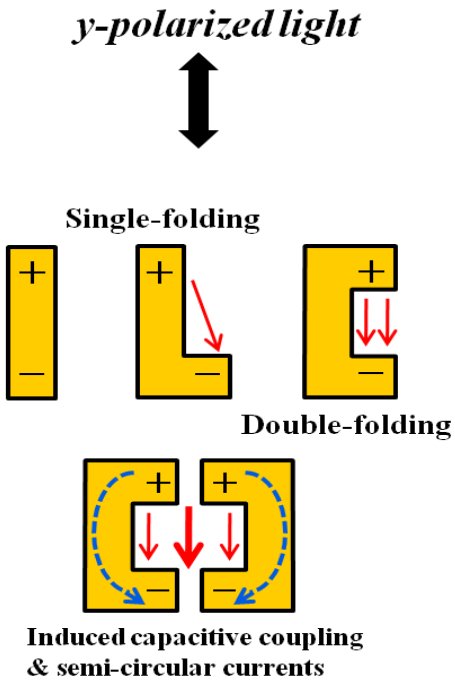

Figure 3.2.4. Charge redistribution model when FFR unit is illuminated by *y*-polarized light. In the vertically-polarized illumination, upper and lower horizontal parts of the single folded rod provide short paths for charge deposits, producing capacitive coupling between them, and the interference between two capacitive couplings in left and right single folded rods dominates the overall response and the far-field radiation of the FFR unit.

Although somewhat different charge distribution and resultant fields are configured as compared with those of the *x*-polarized light illumination, we can expect quite similar current flows (and thus, a similar far-field radiation pattern) in this *y*-polarized incident light. Therefore, contrary to the conventional monopole metal rod or coupled nano-rods in which the strong radiations occur only when the incident polarization direction is along their major axis, the radiations from the FFR unit can be regarded as quasi-polarization-insensitive.

3.3. Optimizing process of faced folded metallic nanorods via numerical analysis

In this section, design methodologies of FFR unit are delineated.

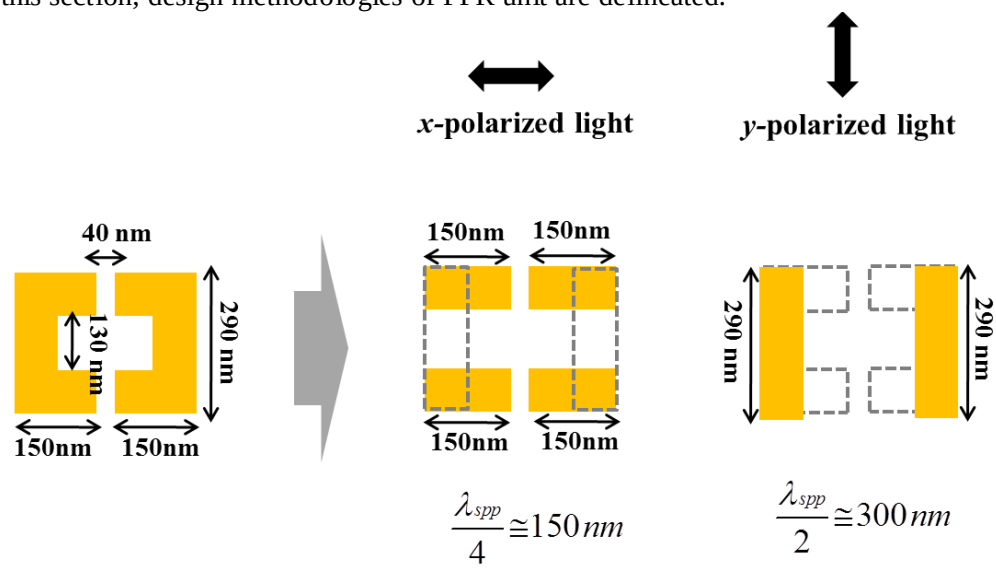

Figure 3.3.1. Design mechanism of plasmonic faced folded metallic nanorods when the incident wavelength is 633 nm. When the FFR unit is illuminated by *x*-polarized light, it can be approximately double coupled metallic nanorods. The length of horizontal metallic nanorod is scaled as $\lambda_{spp}/4$. The length of vertical metallic nanorod is scaled as $\lambda_{spp}/2$.

To design the shape and determine the physical dimensions of FFR unit, there are two important factors to be addressed. First one is how to scale the length in vertical and horizontal parts in FFR unit. As mentioned in Section 3.2, the effective modeling of FFR unit is differentiated by incident polarization state of light. When the incident light is *x*-polarized light, FFR unit is effectively approximated by double coupled metallic nanorods. The length of metallic nanorods is chosen from $\lambda_{spp}/4$, which is previously described in Section 2.1.4. Hence, the effects of localized surface plasmons are dominant in FFR unit when illuminated by *x*-polarized light. On the other hand, it is not identical when illuminated by *y*-polarized light. The FFR unit illuminated by *y*-polarized light can be approximated to two vertical rods. In this proposed FFR unit, the length of

vertical part is set to 290 nm, which is close to the value of $\lambda_{spp}/2$ but not identical. It is not the same manner to explain the design mechanism of FFR unit. But, there are certain issues to determine the vertical length of FFR unit. One of major difference is folded structure which leads to give rise to "*folding effect*". The best folding degree is necessary to allow the FFR unit to optimize in visible regime. Therefore, the point of comprise should be found out.

The degree of folding in a metallic nanorod can be associated with the induced charge redistribution mechanism in FFR unit. In perspective, there are two cases to be addressed when illuminated by *x*-polarized light, presented in Fig. 3.3.2. First one in Fig. 3.3.2 (a)-(c) is that the vertical length of a single metallic folded rod is 190 nm. It is shorter than the proposed dimension of FFR unit and more folded. Second one is that the vertical length of a single metallic folded rod is 340 nm. It is longer than the proposed dimension of FFR unit and less folded. As shown in Figs. 3.3.2 (a)-(c), electric field distribution and surface current flow in shorter FFR unit are similar distribution with those of double coupled nanorods. Capacitive couplings are not observed in shorted FFR unit. That is why the shorter FFR unit looks like double coupled nanorods. It does not have unique properties of proposed FFR unit. On the other hand, as the vertical length of a single metallic folded rod is longer, the brighter spots at the edges are observed. Surface current flow goes more to the edges of longer FFR unit. It implies that more charge nodes are produced in Figs. 3.3.2(d)-(f). If the vertical length of FFR unit is long enough, it seems to have the resonant behavior by itself.

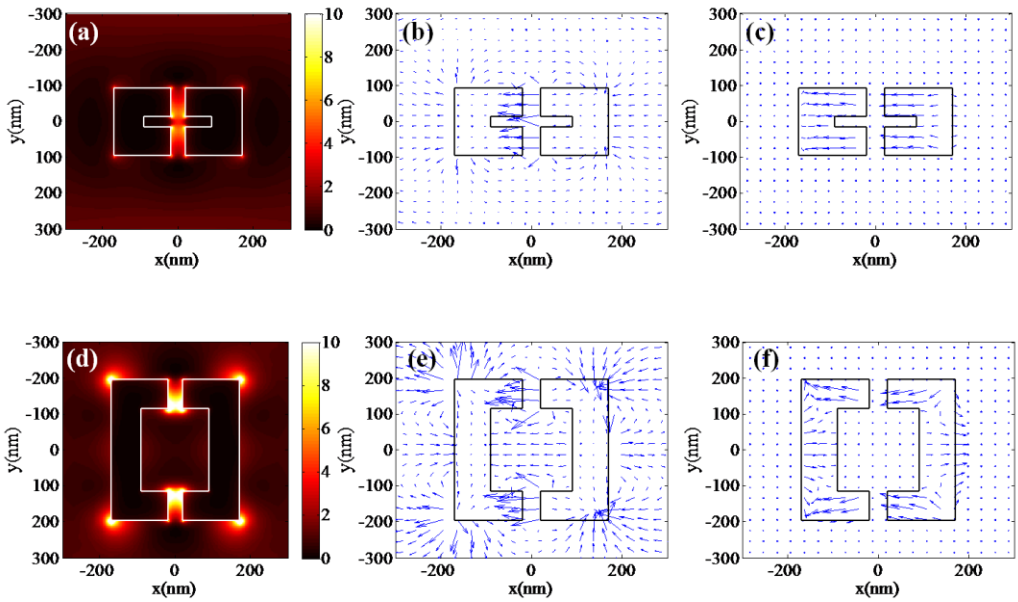

Figure 3.3.2. (a) Intensity, (b) magnitude/direction of the electric fields inside the 190 nm vertical length of FFR unit (z = 65 nm) at a specific phase at which the capacitive electric fields across two narrow gaps are maximized, and (c) distribution of the current flows at the top surface of the shorter FFR unit at π / 5 after the phase used in (b). Note that it takes about π / 5 for the electric field shown in (b) to reach the top surface. (d) Electric field intensity of 340 nm vertical length of FFR unit, (e) magnitude/direction of the electric fields inside longer FFR unit (z = 65 nm) at a specific phase at which the capacitive electric field across two narrow gaps are maximized, and (f) distribution of the current flows at the top surface of longer FFR unit. From (a) to (e), the illuminating light is *x*-polarized.

However, in case of longer FFR unit, it has a polarization-sensitive problem. One of major characteristics in proposed FFR unit is quasi-polarization-insensitive. Therefore, longer FFR unit cannot represent the optical response of proposed FFR unit.

According to Fig. 3.3.3, induced charge redistribution model is keenly dependent on the vertical length of FFR unit. As mentioned above, semi-circular current flow can be achieved in case that the vertical length of FFR unit is 290 nm. In other words, semi-circular current flow is necessary to be FFR unit as quasi-polarization-insensitive. Therefore, the 290 nm vertical length of FFR unit can be the optimal value in this given geometry.

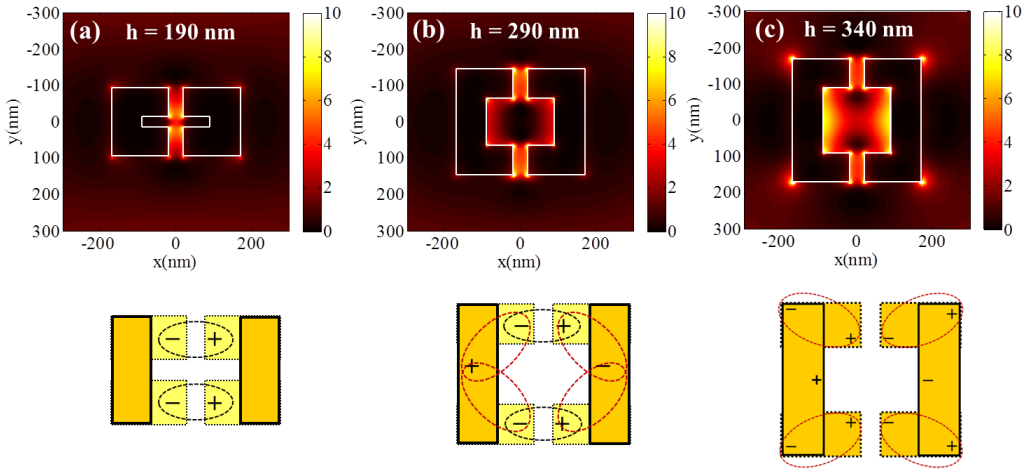

Figure 3.3.3. Induced charge redistribution model when FFR units are illuminated by *x*-polarized light. The vertical length of the folded rod is (a)190 nm, (b)290 nm, and (c)340nm, respectively.

In the other point of view, similar metallic nanostructures should be compared for the sake of optimizing the geometry. Numerical comparisons among metallic rectangular nanostructures, FFR unit, and a metallic rectangular nanoring with bisymmetric four nanogaps are carried out. First of all, the cross-sectional plot of electric field distribution along the *x*-axis in the middle depth z = 65 nm is presented in both metallic rectangular nanostructure and faced folded metallic nanorods in Fig. 3.3.4. At the 40 nm localized nanogap, enhanced electric field distribution is observed due to capacitive coupling. Another interior 130 nm nanogap which is formed by facing two folded metallic nanorods each other is attributed to capacitively couple electric fields from either side of rods. Sharp edges and folded region of a single folded metallic nanorod are associated with the induced charge redistribution path when illuminated by incident light with the wavelength of 633 nm. However, enhanced electric field distribution is only observed in the sharp edges of metallic rectangular nanostructure. It depends on the aspect ratio of a metallic rectangular nanostructure, which is associated with the depolarization factor.

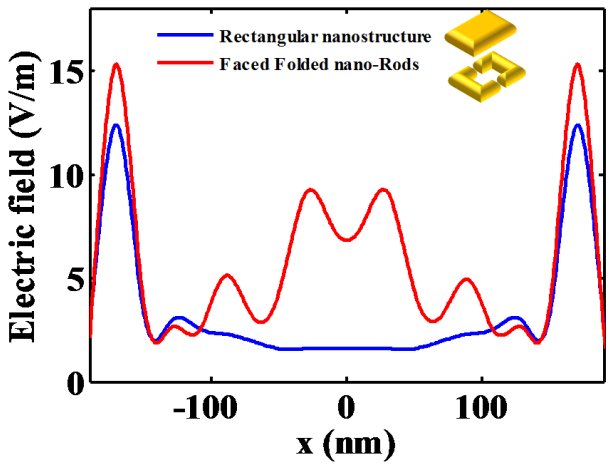

Figure 3.3.4. One-dimensional cross-sectional plot of electric field distribution for metallic rectangular nanostructure and faced folded nanorods. Simulated structures are centered along the *x*-axis (at the middle depth z = 65 nm).

Hence, it can be said that FFR unit possesses multiple locations to boost the localized field strength. To validate the FFR unit as a competitive metallic nanostructure, more numerical comparisons are shown. The plots of local maximum electric field changing the wavelength of incident light in three nanostructures are calculated in Fig. 3.3.5 (a). This graph illustrates that the maximum localized field value is observed at the FFR unit around the wavelength of 633 nm. As presented in Fig. 3.3.5 (b)-(d), the electric field intensity distribution of the FFR unit is brighter than any other two cases at the localized two nanogaps in the same intensity scale. According to these comparisons, it can be said that the FFR unit seems to be optimally designed in visible range.

According to the calculated spectra, the optimal resonant wavelength of metallic rectangular nanostructure is approximately the wavelength of 650 nm. The horizontal length of a metallic rectangular nanostructure is in the vicinity of $\lambda_{spp}/2$ when the incident wavelength is 650 nm. In other words, the resonance of metallic rectangular nanostructure follows the surface plasmon resonance. The optical resonant wavelength in

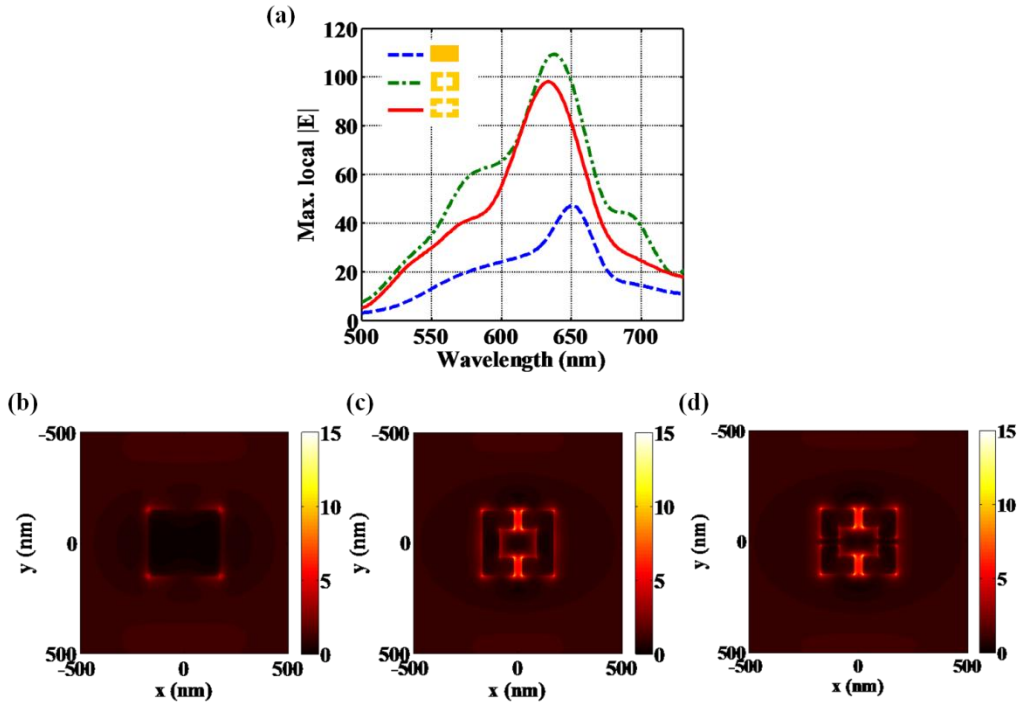

Figure 3.3.5. Comparisons of faced folded metallic nanorods with metallic rectangular nanostructure and metallic rectangular nanoring with bi-symmetric nanogaps are performed. (a) plot of maximum field value factor, changing the wavelength of incident light. Electric field intensity distributions of (b) a metallic rectangular nanostructure, (c) faced folded metallic nanorods, and (d) a metallic rectangular nanoring with bisymmetric four nanogaps at z = 120 nm. Incident light is x-polarized and the magnitude of incident electric field is 1 (V/m).

both FFR unit and metallic rectangular ring is near the wavelength of 633 nm. The horizontal length in either side of each nanostructure is 150 nm, which approximately corresponds to $\lambda_{spp}/4$. These numerical results also insinuate that resonant behavior is relevant to perimeter resonance and then the capacitive coupling arisen from localized nanogaps is attributed to non-resonant effect. In both polarization state of light including x- and y-polarized light, the optimal resonant wavelength in FFR unit strongly coincides with the surface plasmon wavelength λ_{spp} .

3.4. Functionality of plasmonic faced folded metallic nanorods: a compact light concentrator

3.4.1. Fabrication and experimental setup

As follows, the functionalities of radiations from the FFR unit are experimentally investigated. The FFR unit is qualified as strong near-field intensity regardless of the incident polarization sate of light via numerical analysis. In this experiment, further exploitation aims to pursue versatile roles of FFR unit such as an optical antenna and light concentration. Hence, it is necessary to identify the near- and far-field optical response emanating from FFR unit. Therefore, the holographic microscopy technique [46, 47] is adopted to obtain a three dimensional reconstruction of the complex wavefronts of optical fields emanating from the FFR unit. The experimental setup is shown in Fig. 3.4.1. The author used a He-Ne Laser with the wavelength of 633 nm as a light source. An FFR unit is placed in a square bare aperture (2 μm × 2 μm) keeping the distance between the FFR unit and the surrounding metallic wall large enough to avoid any coupling between them as demonstrated in Fig. 3.4.2. The 130-nm Au layer on the SiO_2 substrate with a 5 nm chromium adhesion layer is prepared with an electron beam evaporator (KVE-3004, Korea Vaccum Corp.). FFR units and surrounding apertures are fabricated with a focused ion beam machine (Quanta200 3D, FEI Corp.). Fabricated samples of a bare aperture and an FFR unit placed in it are shown in Fig. 3.4.3 (a) and Fig. 3.4.3 (d), respectively.

To experimentally demonstrate the behavior of FFR unit as a compact light concentrator and plasmonic antenna, the far-field probing was performed by the use of holographic microscopy. In digital holographic microscopy, the interference patterns are recorded on a CCD camera. The method on probing the generated optical field by the use of holographic microscopy is briefly addressed. Light waves from a coherent source are separated into two arms: One carries information on the optical far-field distribution emanating from an object (e.g., an FFR unit), and the other undergoes stepwise phase shifts. By the use of four-step phase-shift interferometry, light paths or far-field

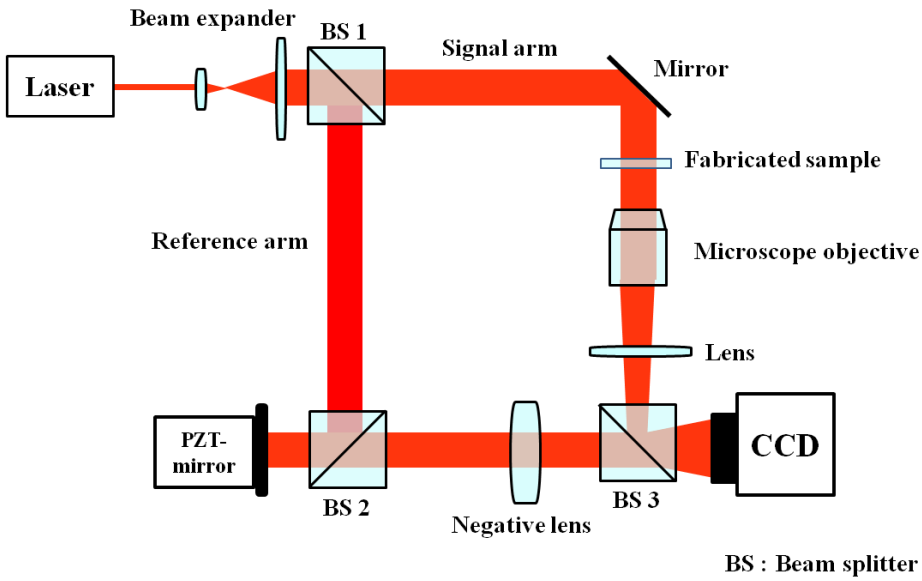

Figure 3.4.1. Experimental configuration adopting the holographic microscopy to measure and reconstruct a three-dimensional distribution of optical fields radiated by the FFR unit.

distributions coming out from the fabricated samples can be effectively retrieved. In our holographic detection, the fabricated structures are placed 20 μm away from the focal plane of the microscope objective so that twin image analysis in the frequency domain can be applied to resolve such phase-shifting errors caused by fluctuations and vibrations during the holographic probing process. The fabricated structures are placed on the motorized linear stage with the translational resolution of 100 nm, and the piezoelectric-driven mirror enabling us to obtain phase-shifting interferograms is controlled by home-made LabVIEW-based software. A negative lens in the reference arm is required to compensate for the wavefront curvature induced by the objective lens in the signal arm, so that the beam profile of the signal wave passing through the objective lens can be equivalent to that of the reference wave. The signal light passing through these structures reaches the CCD camera (XCD-SX90, Sony Corp.) via a 100 x microscope objective (MPlanApo, Olympus Corp., NA 0.85). The reference beam undergoes phase shift whose amount is controlled by a piezoelectric-driven mirror. We can reconstruct the three-

dimensional map of the signal light emanating from the FFR unit through a convolution form of the Fresnel transform [48].

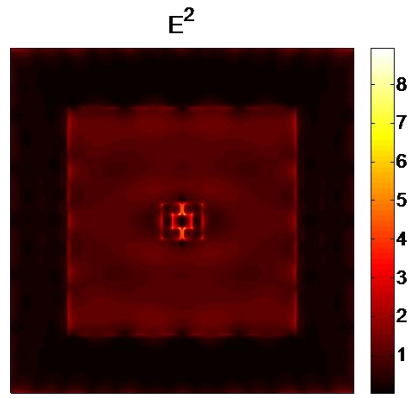

Figure 3.4.2. Numerical electric field intensity distribution at 10 nm above FFR unit placed at the center of bare aperture. It notifies that the field coupling between FFR unit and bare aperture does not almost exist. This result supports the assumption for the fabrication of this sample.

3.4.2. Experimental results via holographic microscopy

The intensities of the transmitted light through a bare aperture and an FFR unit in an aperture are presented. We note that all the plotted intensities are normalized with respect to the same value, i.e., the maximum among the results of all measured figures before normalization. In Figs. 3.4.3 and 3.4.4, we can find that the transmitted light seems to be focused at $z \sim 2$ μm, and then spreads. The simple calculations based on the Fresnel diffraction theory [49] showed similar patterns to these results. Therefore, this focusing and spreading pattern, we can say, results from the diffraction of light through the square aperture. Let us see both Figs. 3.4.3 and Fig. 3.4.4 where the transmitted light intensities through the FFR unit are plotted. It is notable that we can record and reconstruct only the propagating components of the signal beam in the holographic microscopy. That is, the near-fields from the sample are neglected in the reconstructed results in given setup. It can identify two kinds of contributions: one is the diffraction through the aperture surrounding the FFR unit and the other the radiations form the FFR unit itself. Due to the

latter, we can discern that the transmission is significantly enhanced. Moreover, the enhanced intensities are localized especially in a certain region (z = 1.5 ~ 3.5 μm). In Fig. 3.4.5, the cross-sectional views of the transmitted light at these longitudinal coordinates are shown. It can be easily found that the transmitted light (or beam) maintains its intensity profile over this region. These results clearly indicate that the FFR unit can act as a field concentrator (along the transverse directions) or a beaming device in the far-field region. As is shown in the previous section, similar semi-circular current flows are formed in the FFR unit regardless of the polarization states of the illumination.

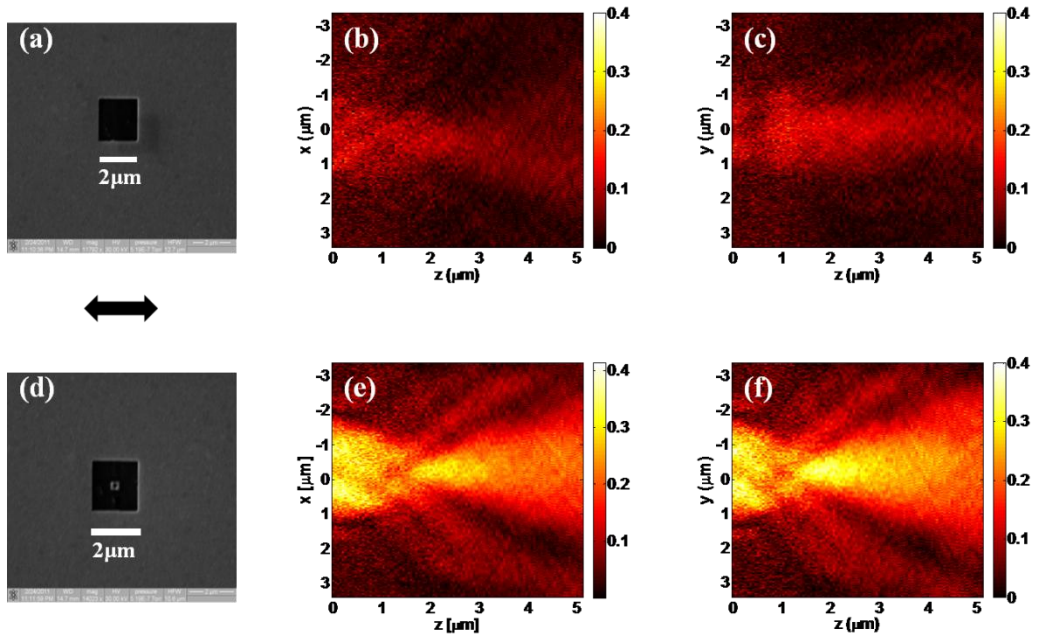

Figure 3.4.3. (a) SEM picture of a fabricated bare aperture (2 μm × 2 μm) and (b), (c) transmitted light intensities through it at y = 0 and x = 0 planes, respectively. In this case, it is not necessary to consider whether the illumination is polarized horizontally or vertically since the aperture is a square. Intensities are normalized with respect to the maximum value among the results of (b), (c), (e), and (f). (d) SEM picture of a fabricated FFR unit placed in an aperture and (e)-(f) transmitted light intensities through it. (e), (f) at y = 0 and x = 0 planes, respectively, when the incident light is polarized horizontally. Intensities are normalized with respect to the maximum value among the all results.

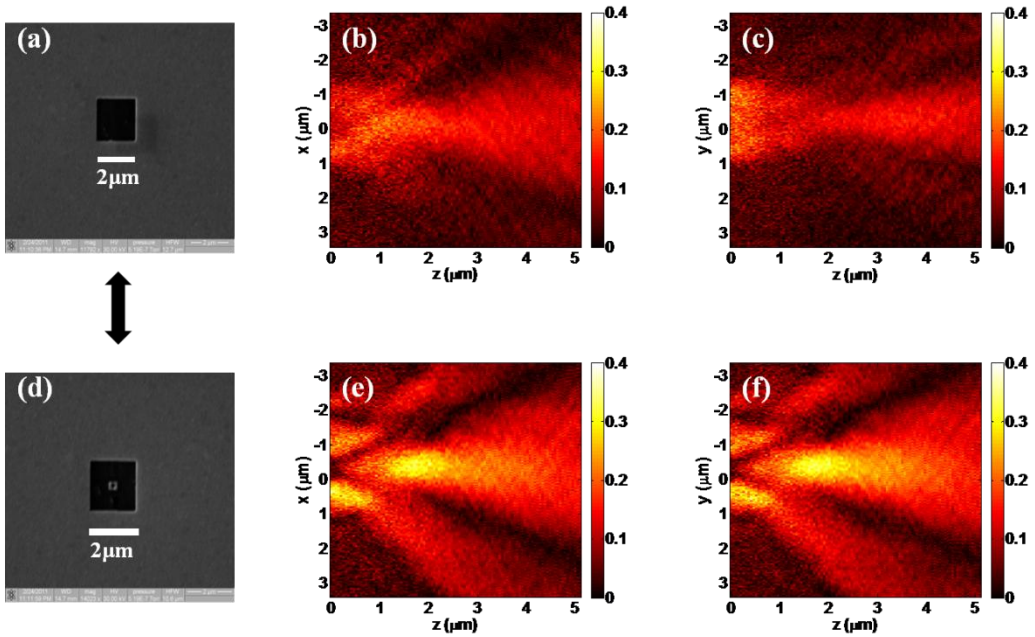

Figure 3.4.4. (a)-(c) the same as Fig. 3.4.3 with vertical polarization. (d) SEM picture of a fabricated FFR unit placed in an aperture and (e)-(f) transmitted light intensities through it for the case of vertically-polarized illumination at $y = 0$ and $x = 0$ planes, respectively. Intensities are normalized with respect to the maximum value among the all results.

Therefore, it can be concluded that much similar far-field radiation patterns regardless of the polarization states as can be found from Figs. 3.3.2 to 3.3.4., meaning that the operation of the FFR unit as a field concentrator can be regarded as quasi-polarization-insensitive.

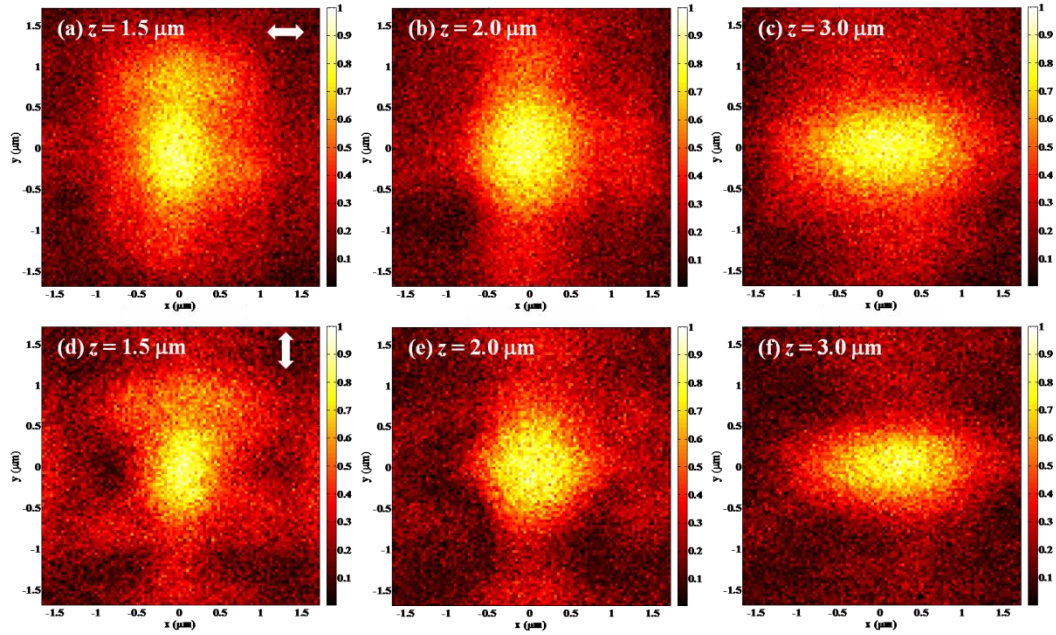

Figure 3.4.5. Cross-sectional view of transmitted light through the FFR unit at various longitudinal (z) positions for (a)-(c) horizontally- and (d)-(f) vertically-polarized incident light.

3.5. The array of FFRs embedded in a metallic nanoslit

Light transmission through a subwavelength metallic slit is considerably diffracted. Aforementioned in the previous section, the FFR unit is a subwavelength metallic nanostructure and can also help to enhance localized electromagnetic field strength. Based on these properties, it can be predicted that the array of FFRs can be attributed to the increase of the transmitted field intensity when embedded in a metallic nanoslit. Two major features of localized surface plasmons arisen from FFR unit can be utilized. One is a highly localized field below diffraction limit and the other is a considerable intense radiation field accompanying to it. It can offer feasible access to manipulate light in attempt to untangle various issues related to weak absorption and radiation efficiency in intensity. In here, the transverse array of FFRs embedded in a metallic slit is proposed to

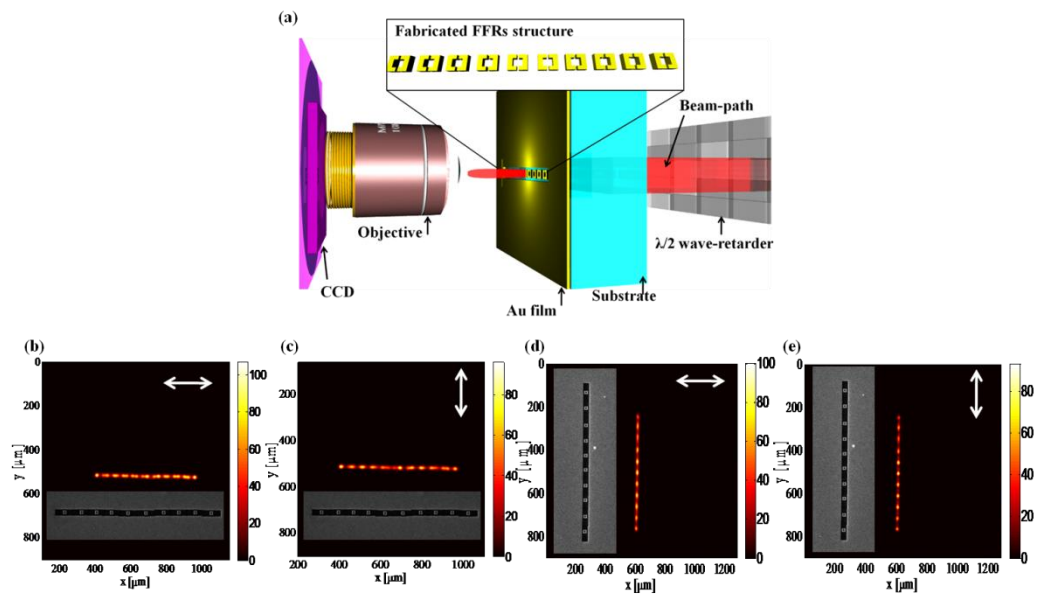

Figure 3.5.1. Optical measurement of the array of FFRs embedded in a metallic slit. **(a)** Experimental configuration via scattering microscopy, (b)-(c) far-field intensity images (a.u) from the transverse array of FFRs when illuminated by horizontally- and vertically-polarized light, (d)-(e) far-field intensity images from the longitudinal array of FFRs when illuminated by horizontally- and vertically-polarized light.

achieve transmission enhancement passing through a given geometry. The dimension of metallic slit is 20 μm horizontal and 0.55 μm vertical. In Fig. 3.5.1, the experimental configuration is briefly illustrated. In an attempt to measure the far-field intensity emanating from the metallic nanoslit embedded by the array of FFRs, 10 FFR units are equally arrayed inside a metallic nanoslit. Since the FFR unit has optimal resonance at the 633 nm wavelength of incident light, He-Ne laser with the wavelength of 633 nm is used as a light source. A half-wave retarder is placed behind the fabricated sample to control the polarization state of light. The microscope objective with the magnification ratio of 100 and with the numerical aperture of 0.85 (MPlanApo, Olympus Corp.) is used to detect the transmitted light, and the charge-coupled device (CCD) with the resolution of 1280 (horizontal) × 960 (vertical) pixels, each size of which is 3.75 μm × 3.75 μm, (XCD-SX90, Sonay Corp.) is used to capture the intensity distribution pattern. Figures. 3.5.1 (b)-(e) show the far-field intensity images given by the array of FFRs embedded in a metallic nanoslit in transverse and longitudinal directions. Transmitted light from the transverse array of FFR units embedded in a metallic slit in Figs. 3.5.1 (b)-(c) is reradiated through the intervals between FFR units when illuminated by horizontally- and vertically-polarized light, respectively. It indicates that far-field intensity reradiated from the array of FFRs embedded in a metallic nanoslit when illuminated by horizontally-polarized light is a little stronger than the far-field intensity obtained from the incidence of vertically-polarized light. In attempt to analyze the physical phenomena, numerical calculations are performed with a RCWA (Rigorous Coupled-Wave Analysis) technique. FFRs are arrayed semi-infinitely inside a metallic nanoslit. Periodic boundary conditions are adopted. Figure 3.5.2 numerically shows the near- and far-field intensity distributions reradiated from the transverse array of FFRs embedded in a metallic nanoslit. When illuminated by horizontally- and vertically-polarized light, respectively, electromagnetic field enhancement between FFR and its adjacent FFRs is observed. In addition, transmitting light from the intervals between the FFR and its adjacent FFRs can propagate to the far-field region. When FFRs are longitudinally arrayed inside a metallic nanoslit, similar coupling phenomenon is observed in Figs. 3.5.1 (d)-(e).

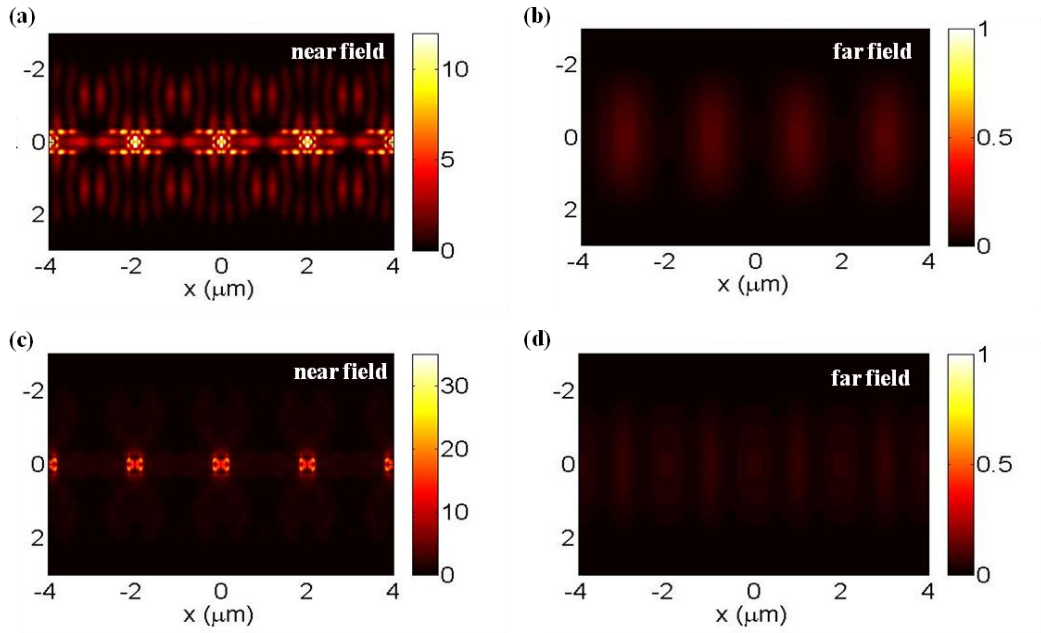

Figure 3.5.2. Numerical intensity distributions (a.u) calculated by RCWA method: (a) Near-field distribution obtained at 10 nm above the transverse array of FFRs and (b) far-field distribution obtained at 10 μm above the transverse array of FFRs when illuminated by horizontally-polarized light. (c) Near-field distribution obtained at 10 nm above the transverse array of FFRs and (d) far-field distribution obtained at 10 μm above the transverse array of FFRs when illuminated by vertically-polarized light.

For the purpose of validating the directionality and comparing a metallic nanoslit, the polar plot of radiation pattern with respect to the array of FFRs embedded in a metallic nanoslit and a metallic nanoslit is introduced in Fig. 3.5.3. According to this plot, far-field radiation pattern given by the transverse array of FFRs points out higher radiation intensity and more directional radiating pattern than the a bare metallic nanoslit. When plasmonic FFR units are arrayed inside a metallic nanoslit, localized far-field transmission enhancement without diffractions is achieved.

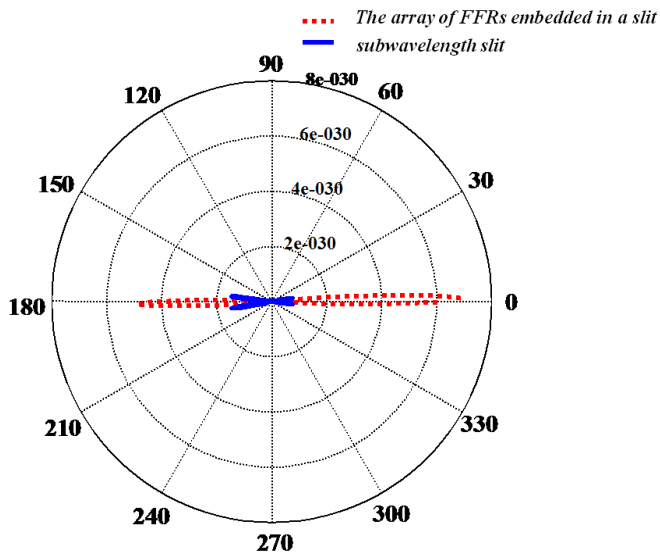

Figure 3.5.3. Polar plot of radiation pattern with respect to a subwavelength metallic slit and the array of FFRs embedded in a subwavelength metallic slit.

Chapter 4

Field enhancement through a nanoslit by the use of metallic nanoislands

4.1. The use of nanoslit in optical range

Recent years have seen a major footstep of research into nano-photonics based on surface plasmon polaritons (SPPs). SPPs are optical-frequency or terahertz electromagnetic waves coupled with collective oscillation of electron plasma in metal. SPPs can be excited under appropriate condition when the light or terahertz wave is incident on the interface between dielectric and the noble metal that has the negative real part of permittivity. They propagate along or become trapped at metal-dielectric interfaces. Electromagnetic waves can be fumbled with metallic nanostructures beyond the diffraction limit with the help of SPPs. For example, various types of metallic nanostructure have been proposed for guiding SPP modes. These contain thin metal film, chains of metal nanoparticles, various shapes of metal nanorods, and nanoholes in a metallic medium, nanogaps between metallic media, and slot waveguides in the form of rectangular nanogaps in thin metal film [50]. Metallic nanostructures can also convert optical radiation into intense, engineered, localized plasmonic field distribution, functioning as plasmonic antennas and lenses [51]. Thus, wherever subwavelength control over light is desired, metallic nanostructures are likely to act as a tangible part. Hence many researches relevant to a subwavelength metallic slit in optical regime have been endeavored for overcoming the diffraction limit [52-54]. Studies on plasmonic beaming [55, 56] and focusing phenomena [57] are some of the key issues in this

research field. Furthermore, a nanoscale metallic slit, also called “nanoslit”, has received much attention and been utilized in wide ranges of plasmonics [58]. A nanoslit can play versatile roles for plasmonic circuits, nano-resolution optical imaging techniques and sensors. It acts as a plasmonic waveguide which transmits the light into confined region. It can also function like a plasmonic antenna so that it enhances near-field intensity or far-field radiation. However, a lot of issues associated with a metallic nanoslit have been remained. Among them, two main issues for a metallic nanoslit are light intensity enhancement through a metallic nanoslit and tuning the resonance condition of metallic nanoslit.

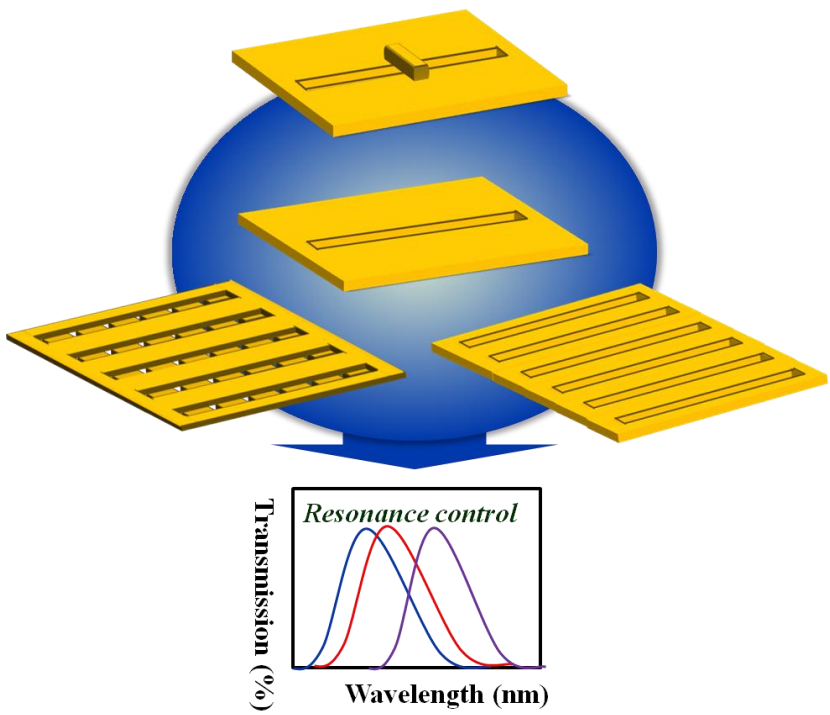

Figure 4.1.1. Various geometries extended from a metallic nanoslit for the purpose of tuning resonance condition of optical characteristics.

Recent researches have reported that resonance conditions through a metallic slit are influenced by resonant metallic nanoparticles placed within the structure or the array of metallic slits in terahertz and optical regime [59-

63] as presented in Fig. 4.1.1. For example, Park *et al.* proposed that when a Pt nanoparticle is placed at the center position on the THz slot antenna, the electromagnetic coupling between the resonances supported by each of the two subwavelength metallic slits begins to unite and give rise to another mode [64]. Since they assumed that THz slot antenna is physically similar to a metallic slit, it provided the route to manipulate the resonant wavelength by controlling the dimension of a metallic slit. Meanwhile, resonant metallic nanoparticles placed within a metallic slit are attributed to the resonance condition as well. It is claimed that transmission spectra show how the size, orientation of the nanoparticles, and the period of the nanoslit array determine the maximum transmission wavelength, the magnitude of the transmission, and full width half maximum (FWHM) of the resonance [65]. In these investigations, transmission of polarized light along the subwavelength slit was studied. But, these publications just provide the effect of resonance conditions with regard to the array of nanoslits, physical parameters of slit, or the position of a nanoparticle upon a slit. The mechanism of field enhancement when metallic nanoparticles or nanoislands are placed within a slit has not been unveiled. Hence, it is of interest to reveal the physics of field enhancement and propose a novel method to boost field intensity passing through a nanoslit.

4.2. Transmission enhancement through a nanoslit by embedded metallic nanoislands

In this section, the pathway to enhance light intensity passing through a metallic nanoslit by embedding metallic rectangular nanoislands is introduced. Assumptions are that the role of an embedded metallic nanoisland can be defined as a charge relocator and resonance shifter in a nanoslit for the intensity enhancement. To demonstrate experimentally, the radiation intensity from the proposed structures for the both polarization states of incident light at the specific wavelength is measured by far-field scattering microscopy. The intensity enhancement originates from induced accumulated charges from the embedded metallic rectangular nanoislands, which are excited from the

incidence of both horizontal and vertical polarizations. In attempt to verify our model, the spectrum of proposed structures with respect to incident polarization is numerically analyzed. The degree of intensity enhancement can be determined by the number and spacing distance of embedded metallic rectangular nanoislands, which will be shown in experimental and numerical results. We also present that the resonance condition of a nanoslit could be tuned by the insertion of metallic rectangular nanoislands for the incidences of both horizontal and vertical polarizations.

4.2.1. Schematic and experimental configuration

Let us precisely describe the experimental configuration and the schematic of proposed structure. Figure 4.2.1 delineates the experimental setup for the measurement of far-field light intensity. The proposed structure is illuminated from the bottom by the laser with the free space wavelength of 660 nm (Newport, LQA660-110C) and the surface plasmon evanescent field intensity distribution was measured by the near-field scanning optical microscope (NSOM) (Nanonics, Multiview 4000). Far-field scattering microscopy equipped with a high numerical aperture (NA) objective (PlanApo, 100x, NA=0.85, Olympus Inc.) is used for far-field optical imaging. The transmitted light after interacting with the proposed structure is collected by an objective of 0.85 NA. We can acquire the microscopic images by a charge-coupled device (CCD) camera. Figure 4.2.1(b) provides the conceptual schematic diagram of the proposed structure. Typically, the transmitted light through a nanoslit is weak without embedded nanoisland. To overcome weak radiation from a nanoslit, metallic rectangular nanoislands are employed as a charge accumulator and relocator at a nanoslit for the enhancement of light intensity passing through a nanoslit. Metallic rectangular nanoislands are placed within a nanoslit $(10\,\mu\mathrm{m}(x)\times 370\,\mathrm{nm}(y))$. The dimension of a metallic rectangular nanoisland is developed from relevant references [66]. The size of the embedded metallic rectangular nanoisland is 340 nm (x) by 290 nm (y).

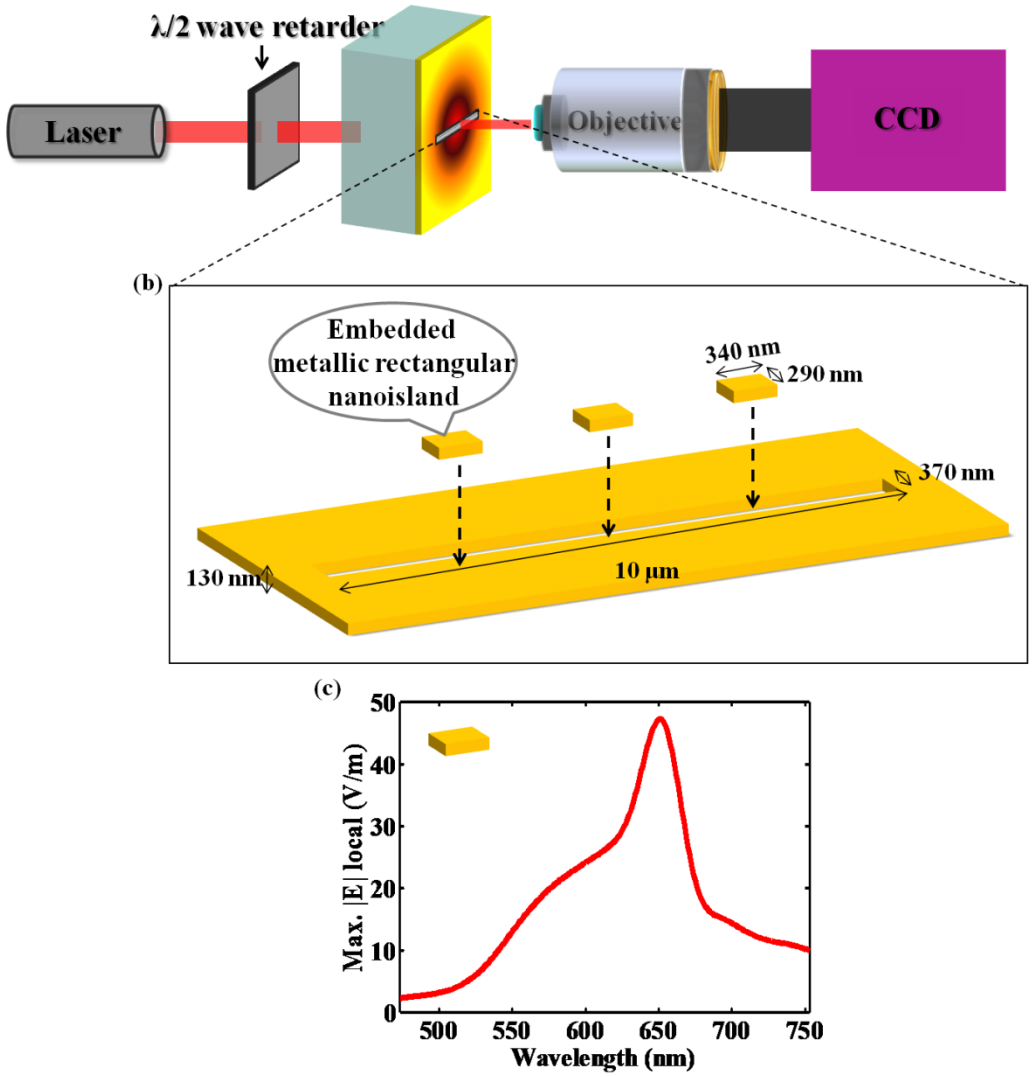

Figure 4.2.1. (a) Experimental setup to measure far-field radiation intensity from the proposed structures. (b) Schematic illustration of the proposed structure. (c) Numerical plot of maximum local electric field values on the top surface of a metallic rectangular nanoisland, changing the wavelength of incident light. The amplitude of incident electric field is 1 (V/m).

The thickness of thin film gold layer and gold rectangular nanoisland is 130nm and glass (n = 1.5) is used as a substrate. The thickness of metallic layer is thick enough to block the incident illuminated light. The thickness of a metallic rectangular nanoisland has been numerically optimized. In order to avoid the effect of thickness difference between thin film metal layer and metallic rectangular nanoisland, the author establishes the identical thickness of thin film metal layer with a metallic rectangular nanoisland. To identify the spectrum of a metallic rectangular nanoisland, the author performed numerical calculations with three-dimensional finite difference time domain (FDTD) method, using the Palik parameters for the permittivity of Au, and assuming normal plane waves incident uniformly. The surrounding environment is assumed to be a vacuum and open boundary condition is used. The numerical plot of maximum electric field with respect to incident wavelength on the top surface of a metallic rectangular nanoisland, which is inserted inside a nanoslit, is exhibited in Fig. 4.2.1(c). As we ascertained in Fig. 4.2.1(c), the maximum field enhancement can be attained near the wavelength of 660 nm, which is equivalent to the wavelength of laser source. Accordingly, we expect to achieve considerable transmission enhancement through the proposed structure.

4.2.2. Experimental results by far-field microscopy and near-field scanning microscopy (NSOM)

To experimentally demonstrate the functionalities of these proposed structures, we fabricated the proposed metallic structures. Electron beam evaporator (KVE-3004) is used for metal deposition onto the glass slide and the patterns are milled by focused ion beam machine. First of all, we investigate the case for the incidence of horizontally-polarized light with respect to a nanoslit in Fig. 4.2.2(a), one metallic rectangular nanoisland at the center of a nanoslit in Fig. 4.2.2(b), and three metallic rectangular nanoislands equally spaced at a nanoslit in Fig. 4.2.2(c). Figures 4.2.2(d) - 4.2.2(f) show the far-field scattering intensity distributions of a nanoslit, one metallic rectangular

nanoisland at the center of a nanoslit, and three metallic nanoislands equally spaced at a nanoslit, which are obtained from the scattering microscopy when illuminated by horizontally-polarized light. They depict that when metallic rectangular nanoislands are embedded at a nanoslit, far-field scattering intensity is more enhanced than that of a simple nanoslit. In particular, Fig. 4.2.2(f) exhibits the strongest far-field scattering intensity, increased up to 2.5 times, which is stronger than the case of Fig. 4.2.2(d). It can be said that, within the scope of our experiment, as the number of embedded metallic rectangular nanoislands increases, the far-field scattering intensity gets stronger.

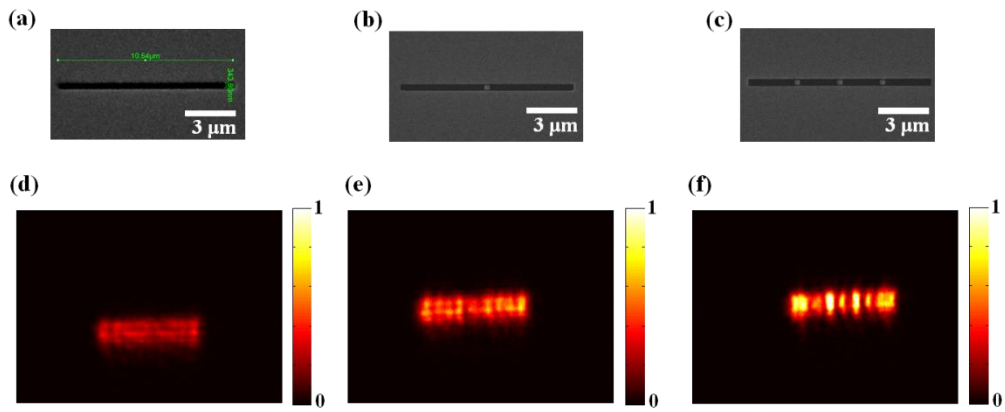

Figure 4.2.2. SEM pictures of (a) a nanoslit, (b) one metallic rectangular nanoisland placed at the center of a nanoslit, and (c) three metallic rectangular nanoislands equally spaced at a nanoslit. (d)-(f) Corresponding far-field scattering intensity profiles obtained from scattering microscopy, when illuminated by horizontally polarized light.

Meanwhile, when the proposed structures are illuminated by vertically-polarized light, far-field scattering intensity is also enhanced in comparison with that of a nanoslit as presented in Fig. 4.2.3. In this case, as the number of embedded metallic rectangular nanoislands increases, we achieve stronger far-field scattering intensity as well. Even though the physical principles are different with regard to the incident polarization state of light, far-field scattering intensity of the proposed structures exhibit almost similar profile regardless of the incident polarization states.

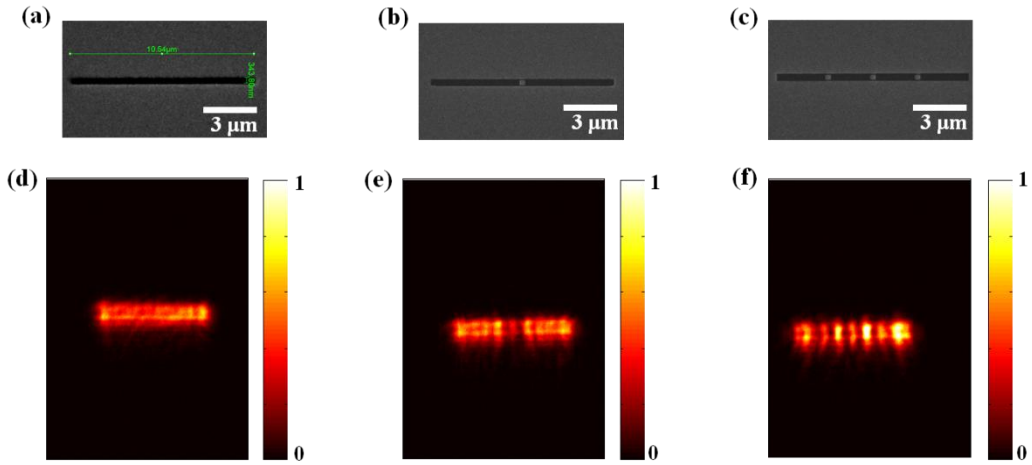

Figure 4.2.3. SEM pictures of (a) a nanoslit, (b) one metallic rectangular nanoisland placed at the center of a nanoslit, and (c) three metallic rectangular nanoislands equally spaced at a nanoslit. (d)-(f) Corresponding far-field scattering intensity profiles obtained from scattering microscopy, when illuminated by vertically polarized light.

In attempt to establish the role of embedded metallic nanoislands inside a nanoslit and examine the near-field profile, the near-field intensity profiles of proposed structures via near-field scanning optical microscopy (NSOM) (Nanonics, Multiview 4000) are measured as shown in Fig. 4.2.4. Near-field intensity profiles show that radiation intensity at the interval between the edge of a metallic nanoslit and embedded metallic rectangular nanoisland is stronger than that above the embedded metallic rectangular nanoisland. In the concrete, the average peak intensity value of cross-sectional intensity plot according to the slit length parallel to the nanoslit of one metallic nanoisland placed at the center of a nanoslit is approximately 0.42. But, the average peak intensity value of cross-sectional intensity plot according to the slit length parallel to the nanoslit of three metallic nanoislands equally spaced at a nanoslit is approximately 0.7. Quantitatively, it makes sense with far-field measured values. Meanwhile, the positions where locally enhanced light intensity is observed are in the vicinity of embedded nanoislands. It means that the source of field enhancement originates from the embedded nanoislands.

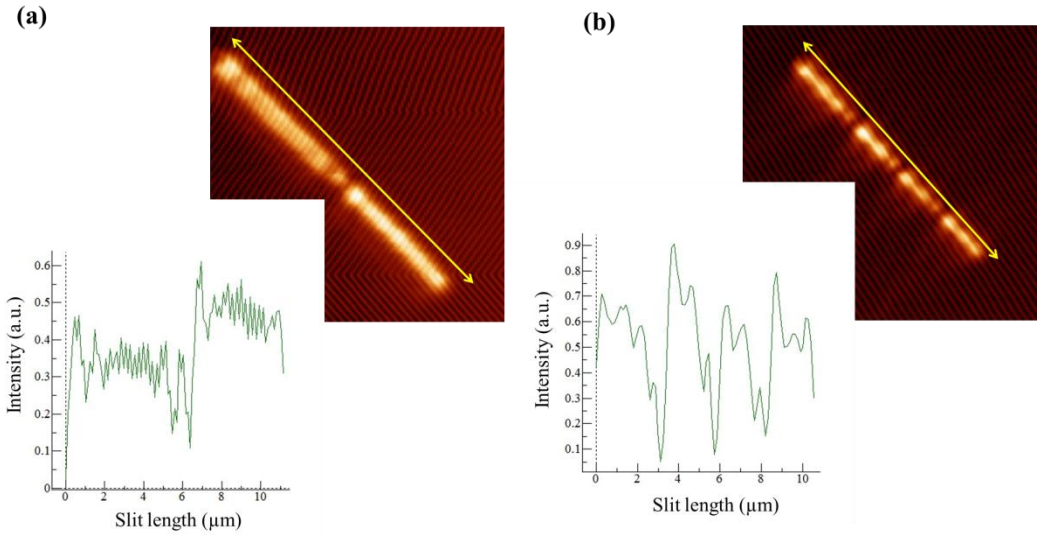

Figure 4.2.4. NSOM image and corresponding cross-sectional intensity plot according to the slit length parallel to the nanoslit of (a) one metallic nanoisland placed at the center of a nanoslit and (b) three metallic nanoislands equally spaced at a nanoslit, respectively, when illuminated by vertically-polarized light.

The far-field intensity profiles show almost the identical profiles as near-field intensity profiles do. Even though this phenomenon cannot be directly explained by the localized plasmon effect of embedded metallic rectangular nanoislands, the increase of far-field scattering intensity would be attributed to near-field enhancement arisen from embedded metallic rectangular nanoislands by the correlation between NSOM images and far-field scattering images [67].

From these experimental results, we can suggest that the near- and far-field intensity passing through a nanoslit can be controlled by the number of embedded metallic rectangular nanoislands.

4.2.3. Theoretical concepts and numerical analysis

To verify and analyze experimental results, we numerically start to examine these proposed structures. Since a nanoslit is used as a reference structure, we should

understand the fundamental characteristics of a nanoslit. Then, the author tries placing one and three metallic rectangular nanoislands inside a nanoslit to clarify not only the role of embedded metallic rectangular nanoislands but also the array effect of embedded metallic rectangular nanoislands. With these structures, the author investigates the optical properties such as enhancement factor and resonance condition by changing the incident polarization state of light: horizontally polarized light and vertically polarized light upon the major axis of a metallic nanoslit.

First of all, the author would like to consider the case when a metallic nanoslit is illuminated by the incidence of horizontally polarized light. Typically, the nanoslit geometry is considered as one of metal-insulator-metal (MIM) plasmonic waveguide structures. The mechanism of SPP excitation in a nanoslit is analogous to the modal analysis of MIM plasmonic structure. The edge effect of a nanoslit can be ignored, assuming that the length of a nanoslit is quite longer than the slit width. For MIM waveguide, both of the transverse electric (TE) and transverse magnetic (TM) modes can be observed. But only some of the TM modes can be called plasmonic modes due to their modal profiles. Plasmonic mode is referred to as a mode which has evanescently decaying model profile both in the metal and dielectric regions. Modes in MIM plasmonic waveguide can be obtained from the Maxwell's equations at the boundary of metal-insulator interfaces. For the symmetrical MIM waveguide, the dispersion relations of the layer system for TM mode can be attained as

$$\frac{\kappa_{x,\,metal}}{\varepsilon_{metal}}+\frac{\kappa_{x,\,air}}{\varepsilon_{air}}\tanh\left(\frac{\kappa_{x,\,air}w}{2}\right)=0,$$
$$\frac{\kappa_{x,\,metal}}{\varepsilon_{metal}}+\frac{\kappa_{x,\,air}}{\varepsilon_{air}}\coth\left(\frac{\kappa_{x,\,air}w}{2}\right)=0, \qquad (7)$$

where κ_x, ε, and w denote the x-directional wavenumber, permittivity of the material, and the width of a nanoslit, respectively. In a similar manner, the dispersion relations for TE mode can be given as

$$\frac{\kappa_{x,\,metal}}{\mu_{metal}}+\frac{\kappa_{x,\,air}}{\mu_{air}}\tanh\left(\frac{\kappa_{x,\,air}W}{2}\right)=0,$$

$$\frac{\kappa_{x,\,metal}}{\mu_{metal}}+\frac{\kappa_{x,\,air}}{\mu_{air}}\coth\left(\frac{\kappa_{x,\,air}W}{2}\right)=0. \tag{8}$$

In this proposed geometry, the width of a nanoslit only allows two plasmonic TM modes and fundamental TE mode. However, TM modes cannot be generated inside the nanoslit due to the incident polarization, which means that only the fundamental TE mode can be allowed to transmit through a nanoslit.

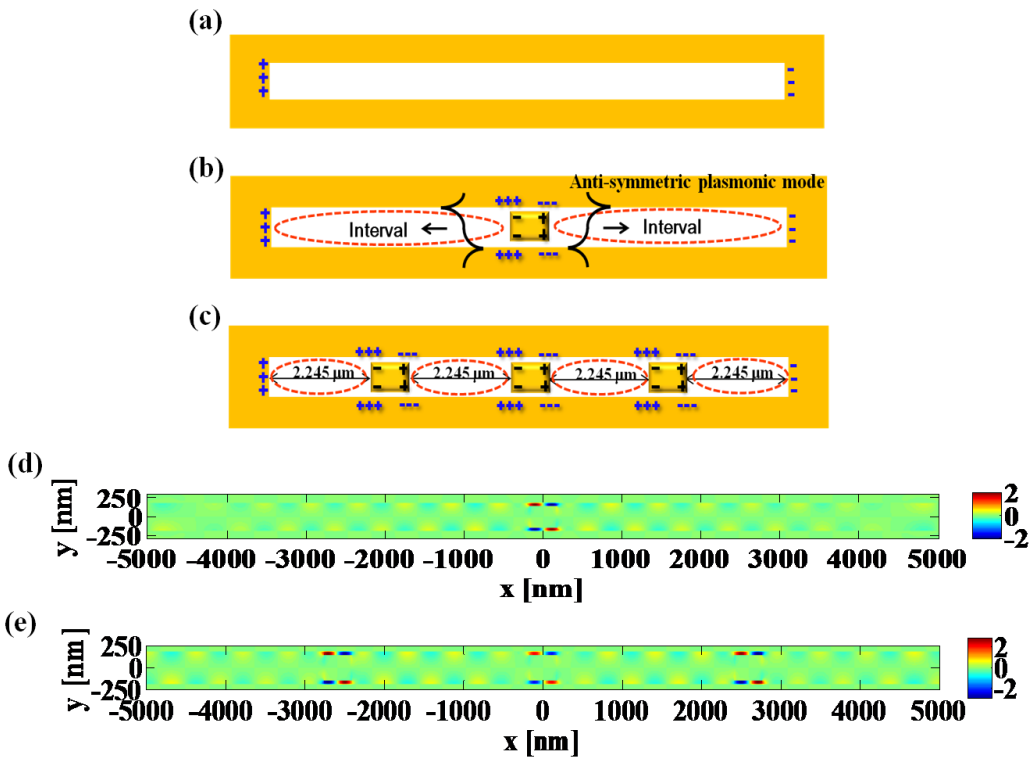

Figure 4.2.5. Charge redistribution model when illuminated by horizontally-polarized light (a) at a metallic nanoslit, (b) one metallic rectangular nanoislands placed at the center of a nanoslit, and (c) three metallic rectangular nanoislands equally spaced at a nanoslit. (d)-(e) Numerical E_y distribution at the middle depth of the nanoslit for the case of one embedded metallic rectangular nanoisland centered at a nanoslit, and three metallic rectangular nanoislands equally spaced at a nanoslit, respectively.

Since fundamental TE mode has only the horizontal component of electric fields, which is normal to the left and right edges of a nanoslit, the fields cannot be considerably changed by the effect from those slit edges. Therefore, we can predict that the field profile inside a nanoslit does not show significant variation along the horizontal direction and the degree of electric field enhancement is not determined by the horizontal length of slit, when we ignore the role of SPPs [68]. Although these aspects cannot be directly adopted in near infrared and visible range, the spectrum of a nanoslit without nanoislands has almost the flat profile, which is shown in Fig. 4.2.6. It indicates that the effect from SPPs in a nanoslit is quite weak to change or enhance the overall spectrum of outgoing fields.

In an attempt to enhance this weak SPPs excitation, we adopt the metallic rectangular nanoisland as a source of SPPs excitation. Figure 4.2.5 describes the induced charge redistribution when one metallic rectangular nanoisland is placed at the center of a

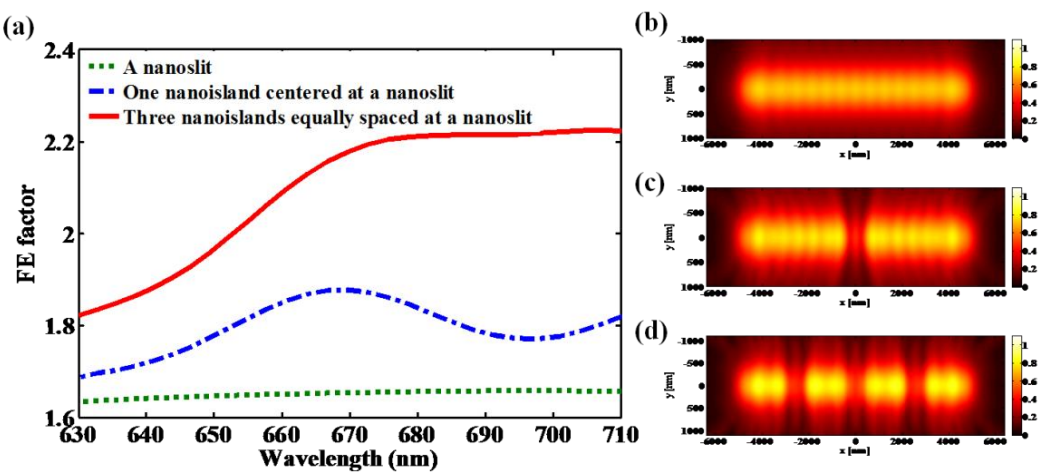

Figure 4.2.6. (a) Their field enhancement factors are shown as a function of incident wavelength of horizontally-polarized light, which is calculated by numerical FDTD method. The amplitude of incident electric field is 1 (V/m). Calculated far-field intensity distribution at (b) a metallic nanoslit, (c) one metallic rectangular nanoislands placed at the center of a nanoslit, and (d) three metallic rectangular nanoislands equally spaced at a nanoslit.

nanoslit. Charges of one metallic rectangular nanoisland are polarized by the incidence of horizontally-polarized light in Fig. 4.2.5 (b). These polarized charges on this embedded metallic rectangular nanoisland attract opposite charges at the rim of a nanoslit near the embedded metallic rectangular nanoisland. Those charges are attributed to certain SPP source that horizontally propagates from the nanoisland, which is referred to as horizontally propagating *anti-symmetric plasmonic mode* as shown Fig. 4.2.5 (d). As compared to the case of a metallic nanoslit (Fig. 4.2.5(a)), *anti-symmetric plasmonic mode* is generated due to the symmetrically induced charges at the rim of a nanoslit resulted from the embedded metallic rectangular nanoisland. In other words, the amount of induced charges in the rim of a nanoslit near the embedded metallic rectangular nanostructure is increased. Additionally, as the number of embedded metallic nanoislands is increased, the amount of induced charges is increased in Fig. 4.2.5 (c). From these effects, it is predicted that field enhancement through the proposed structure can be achieved. In addition, the effect of SPPs from the embedded metallic rectangular nanoisland inside a nanoslit is visualized in Fig. 4.2.5 (d)-(e). The *y* component of electric field distribution explicitly manifests the horizontally propagating *anti-symmetric plasmonic mode* generated from one metallic rectangular nanoisland centered at a nanoslit. These numerical results imply that the use of embedded metallic nanoislands is associated with the field intensity enhancement through a nanoslit in the incidence of horizontally-polarized light.

In order to prove our theoretical approaches, we numerically examine total electric field integrated by effective area to measure the overall enhancement of electric field intensity. To evaluate the degree of field enhancement via the proposed structure, the author defines FE factor as field enhancement factor, when the magnitude of incident electric field is 1(V/m). Figure 4.2.6 (a) reveals that FE factor (which is calculated by the electric field intensity integrated at 100 nm above the proposed structures along the axis of propagation in *x-y* plane, then divided by the open area of proposed structure) is increased more in the proposed structure than that of a nanoslit over the calculated wavelength range. Placing metallic rectangular nanoisland inside a nanoslit lets the

surface charge of a metallic nanoslit more polarized. Furthermore, FE factor of one metallic rectangular nanoisland placed at the center of a nanoslit is a little higher between 660 nm and 680 nm. The reason intuitively comes from the resonance condition of embedded metallic rectangular nanoisland. As mentioned above, the metallic rectangular nanoisland has its own resonance near 660 nm. From these numerical results, we can recognize that localized surface plasmon resonance is obtained from the embedded metallic rectangular nanoisland and contributes to enhancement of FE factor. On the other hand, FE factor at a nanoslit without nanoislands inside it is almost constant as a function of incident wavelength. In Fig. 4.2.5(c), three metallic rectangular nanoislands are equally spaced in a nanoslit. In comparison with Fig. 4.2.5(b), the number of embedded metallic rectangular nanoislands is increased from one to three. The author hypothesizes that the more embedded metallic rectangular nanoislands are placed, the more extra charges are generated. We can confirm that Fig. 4.2.6(a) numerically shows the higher FE factor at the third structure than any other structures. This means that the total scattering fields can be determined by the number of embedded metallic rectangular nanoislands. Far-field intensity distributions emanating from given geometries are also calculated via total scattering fields as shown in Fig. 4.2.6 (b)-(d). Three metallic rectangular nanoislands equally spaced at a nanoslit radiates stronger far-field intensity than any other cases, especially a metallic nanoslit. These numerical far-field results can also coincide with the corresponding experimental results.

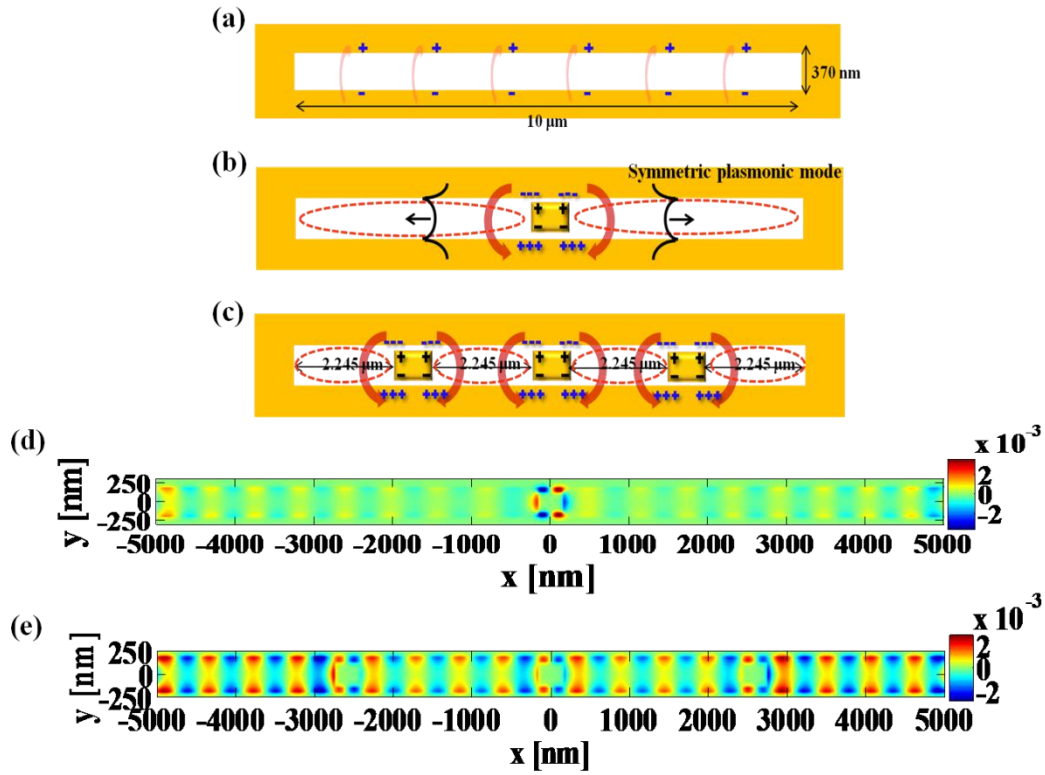

Figure 4.2.7. Charge redistribution model when illuminated by vertically-polarized light (a) at a metallic nanoslit, (b) one metallic rectangular nanoislands placed at the center of a nanoslit, and (c) three metallic rectangular nanoislands equally spaced at a nanoslit. (d)-(e) Numerical H_z distribution at the middle depth of the nanoslit for the case of one embedded metallic rectangular nanoisland centered at a nanoslit, and three metallic rectangular nanoislands equally spaced at a nanoslit, respectively.

By the way, when vertically-polarized light is illuminated, we contemplate different optical phenomenon in the proposed structure. In opposition to the case for the incidence of horizontally-polarized light, only the fundamental TM mode is launched at the proposed structures for the normal incidence. Due to the finite length of nanoslit, this fundamental TM mode inside nanoslit has small modulation along horizontal direction and it makes weak resonant characteristics as shown in Fig. 4.2.8 (a) (green dotted line). Similar to the case of horizontal incidence, placing the metallic rectangular nanoisland inside a nanoslit leads to generation of the horizontally propagating plasmonic modes.

The charge redistribution model can be described as the horizontally propagating *symmetric plasmonic mode* in Fig. 4.2.7.

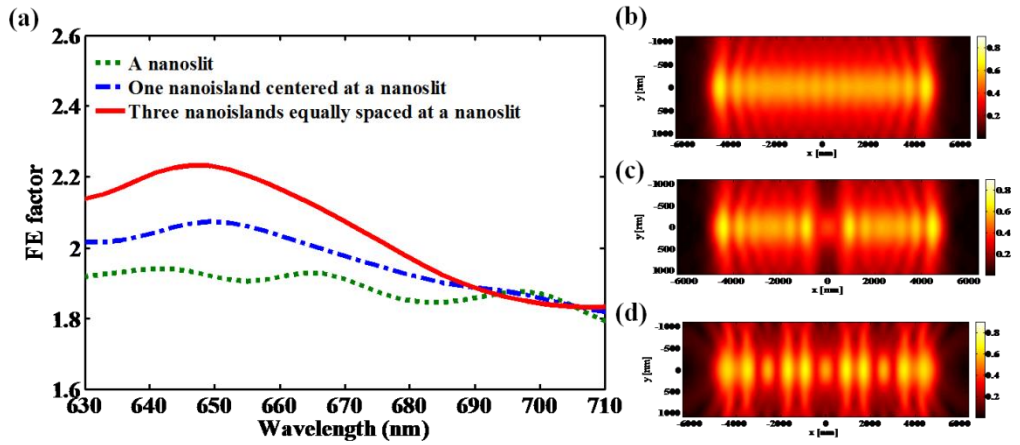

Figure 4.2.8. (a) Their field enhancement factors are shown as a function of incident wavelength of vertically-polarized light, which is calculated by numerical FDTD method. The amplitude of incident electric field is 1 (V/m). Calculated far-field intensity distribution at (b) a metallic nanoslit, (c) one metallic rectangular nanoisland placed at the center of a nanoslit, and (d) three metallic rectangular nanoislands equally spaced at a nanoslit.

Figure 4.2.8 (a) indicates that FE factor periodically responds as a function of incident wavelength in a nanoslit. However, the FE factor between 630 nm and 690 nm is a little bit stronger in the case of one metallic rectangular nanoisland embedded in a nanoslit. In addition, the peak position of FE factor is shifted to shorter wavelength. It can be said that both field enhancement and peak shift would result from the plasmonic resonance of the embedded metallic rectangular nanoisland. The resonant wavelength of embedded metallic rectangular nanoisland is near 633 nm as previously presented in Fig. 4.2.1(c), which belongs to the range between 630 nm and 690 nm. That is why the incident wavelength of laser source belongs to the enhanced wavelength regime of FE factor. Although we cannot directly observe LSPR from the embedded metallic nanoisland in a nanoslit on the incidence of vertically-polarized light, non-resonant effects from the nanogap formed between a nanoslit and a metallic rectangular nanoisland can also be used to further enhance field intensity [69]. A more physical interpretation attributes the enhanced fields to the build-up of opposite charges across the gap. We also identify that

the resonance is enhanced from the embedded metallic rectangular nanoisland centered at a nanoslit on the incidence of vertically-polarized light (as we called horizontally propagating *symmetric plasmonic mode*) in Fig. 4.2.7 (d)-(e). Here, we show the *z* component of magnetic field distribution to verify the horizontally propagating symmetric plasmonic mode generated from a nanoisland, instead of *y* component electric field for filtering the incident field just in the case of vertically-polarized light. In a similar manner, we recognize that when three metallic rectangular nanoislands equally spaced at a nanoslit are illuminated by vertically-polarized light, the strongest field enhancement is attained (Fig. 4.2.8 (a)) as the case for the incidence of horizontally-polarized light. Furthermore, far-field intensity distributions emanating from given geometries illuminated by vertically-polarized light are shown in Figs. 4.2.8 (b)-(d) as well. Those are also identical with experimental results on the incidence of vertically-polarized light.

From this numerical analysis, we can establish that observed experimental results agree with the numerical results. Consequently, we can obtain intensity enhancement passing through a nanoslit, which involves embedded metallic rectangular nanoislands, accompanying with the shift of resonant wavelength arisen from embedded metallic rectangular nanoislands. Additionally, we figure out different physical principles with regard to the incident polarization state of light.

4.2.4. Effects of spacing distance between embedded nanoislands and role of embedded nanoislands in a nanoslit

In previous section, the effects on the number of embedded nanoislands in a metallic nanoslit are explicated. However, there are still remaining perplexing riddles. Spacing distance between embedded metallic nanoislands in a metallic nanoslit is one of hidden parameters to determine either the degree of transmission enhancement or the location of local enhanced spot. For the purpose of disclosing the effects of spacing distance in given

structure, three metallic nanoislands embedded in a metallic nanoslit with 40 nm spacing distance are numerically and experimentally examined as presented in Fig. 4.2.9.

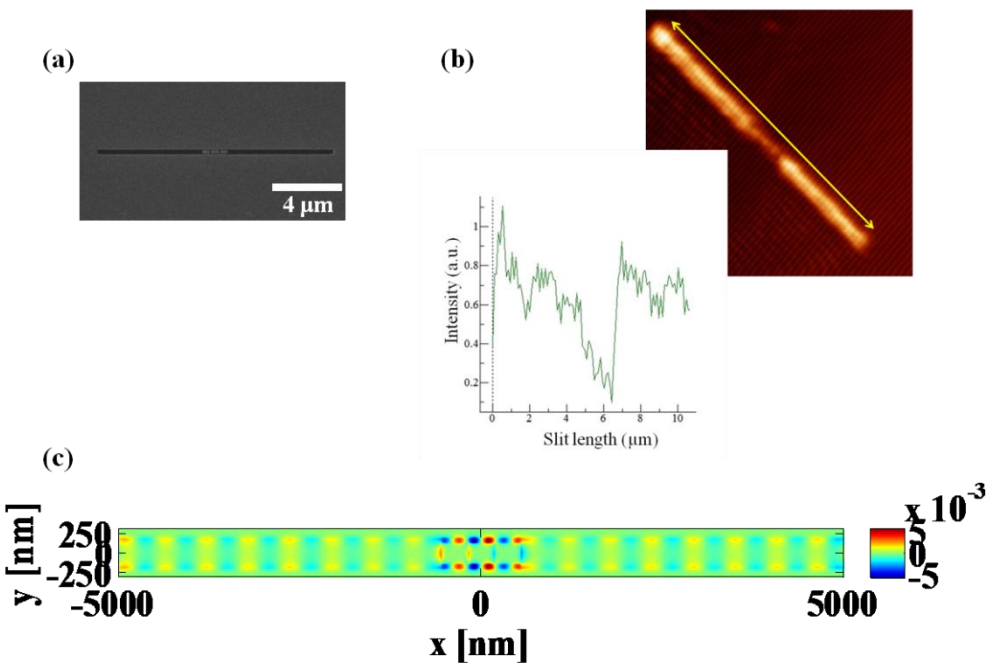

Figure 4.2.9. (a) NSOM image, (b) corresponding intensity plot according to the slit length parallel to the nanoslit and (c) numerical H_z distribution at the middle depth in three metallic nanoislands embedded at a nanoslit with 40 nm spacing when illuminated by vertically-polarized light.

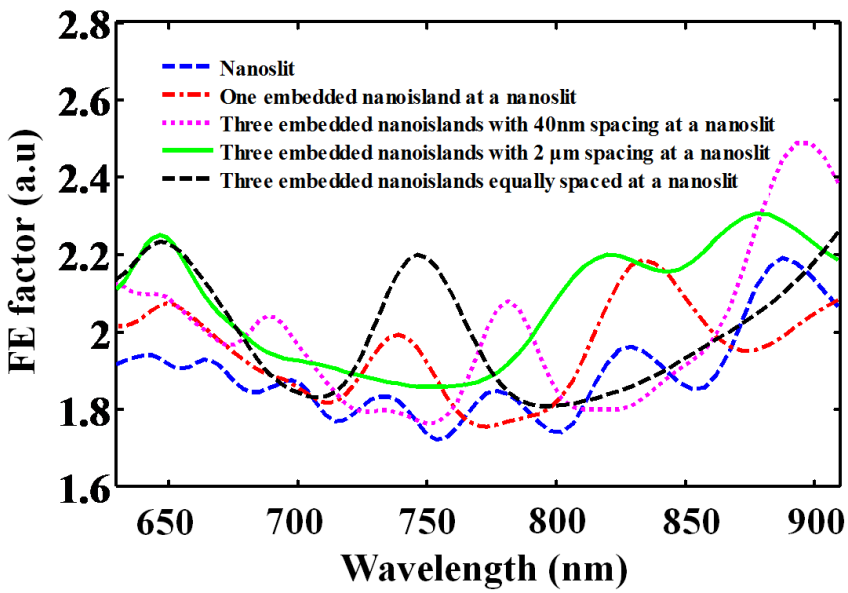

Figure 4.2.10. Field enhancement factors as a function of incident wavelength of vertically-polarized light are presented, extended in wavelength range up to 900 nm, near infrared regime. The cases of three embedded nanoislands with 40 nm spacing and 2 μm spacing at a nanoslit are included.

In previous section, FE factors are examined as a function of incident wavelength only at visible range. In Fig. 4.2.10, FE factors as a function of incident wavelength are numerically plotted including three nanoislands embedded at a nanoslit with 40 nm and 2 μm spacing spacing in visible and NIR regime on the incidence of vertically-polarized light. In case of a metallic nanoslit, fundamental TM modes are periodically observed in visible and NIR regime. When one metallic nanoisland is placed at the center of a metallic nanoslit, one or some of fundamental TM modes are blocked at the location of nanoisland. However, embedded metallic nanoislands are placed inside a metallic nanoslit and then generate a symmetric plasmonic mode as an extra plasmonic mode. The FE factor plot as a function of incident wavelength in three nanoislands embedded at a nanoslit with 40 nm spacing is similar with the case of one metallic nanoisland centered at a nanoslit. Since 40 nm spacing distance is unrecognizable for the wavelength, three nanoislands centered at a nanoslit with 40 nm spacing distance look like one longer nanoisland centered at a nanoslit. According to both Figs. 4.2.5 (d) and 4.2.9 (c),

symmetric plasmonic mode arisen from embedded nanoislands is approximately similar. On the other hand, the plot of FE factor as a function of wavelength in three nanoislands equally spaced at a nanoslit is analyzed with the view of the plasmonic waveguide. When three nanoislands are equally spaced at a nanoslit, some of fundamental TM modes are blocked at three locations of embedded nanoislands. It means that fundamental TM modes from a metallic nanoslit are more blocked than the case of one nanoisalnd centered at a nanoslit. However, the spacing intervals between embedded nanoislands receive more plasmonic modes from both sides of embedded nanoislands and the optimal FE factor value is found near the resonant wavelength of embedded nanoisland at the wavelength of 660 nm. That is why the FE factor of three nanoislands equally spaced at a nanoslit is higher than any other cases. The case of three embedded nanoislands with 2 μm spacing at a nanoslit exhibits similar behavior with the case of three nanoislands equally spaced at a nanoslit.

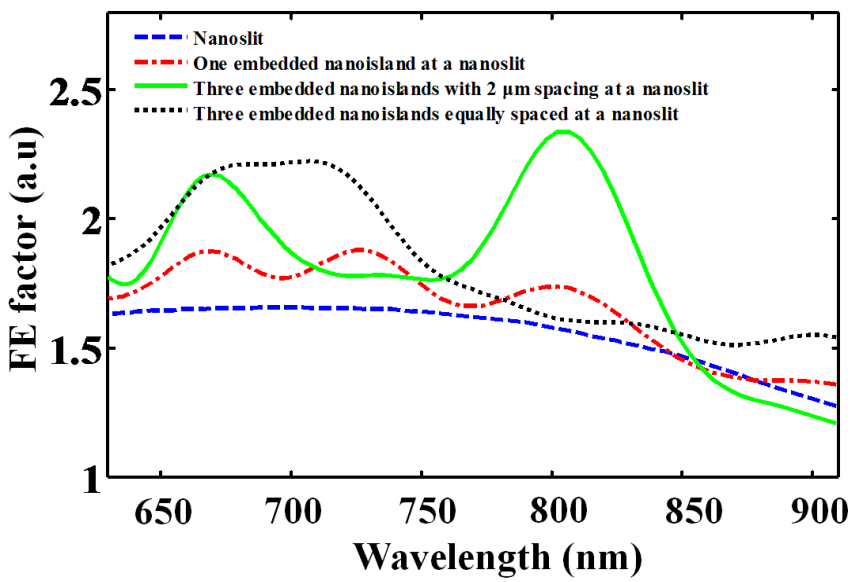

Figure 4.2.11. Field enhancement factors as a function of incident wavelength of horizontally-polarized light are presented, extended in wavelength range up to 900 nm, near infrared regime. The case of three embedded nanoislands with 2 μm spacing at a nanoslit is included.

When illuminated by horizontally-polarized light in Fig. 4.2.11, the role of embedded nanoislands is obviously recognized. A metallic nanoslit does not have plasmonic mode on the incidence of horizontally-polarized light as previously mentioned. According to this plot, the effect of anti-symmetric plasmonic mode from embedded nanoislands is observed in visible and near infrared regime. The case of three nanoislands equally spaced at a nanoslit on the incidence of horizontally-polarized light has the same manner as that on the incidence of vertically-polarized light. The spacing distance between embedded nanoislands can be the crucial parameter to determine the degree of enhancement factor and resonance locations according to the comparison between the case of three nanoislands equally spaced at a nanoslit and the case of three embedded nanoislands with 2 μm spacing.

As a consequence, a novel method to enhance light intensity passing through a nanoslit by employing embedded metallic nanoislands is demonstrated via far-field scattering microscopy and near-field scanning microscopy. The unique characteristics of the proposed structure are numerically explicated with regard to the polarization state of light. It can be said that embedded metallic rectangular nanoisland can act as a charge relocator, SPP source, and resonance shifter in a nanoslit. These properties allow the proposed structure to achieve transmission enhancement. Therefore, we believe that the proposed structure can be dedicated to the development of optical data storage, multiplexed plasmonic biosensors, and novel nano-photonics devices.

Chapter 5

Summary and Conclusion

The dissertation aims to study and develop a metallic nanostructure in optical regime with the mechanism of induced charge redistribution for the light field enhancement, concentration and manipulation. For the fundamental understandings, the optical properties of a metallic nanoparticle are investigated. Major factors are addressed for the purpose of enhancing light field intensity emanating from a metallic nanostructure: LSPR, localized nanogaps explained by local capacitor model, and the analogy with microwave antenna. Associated with diverse approaches, plasmonic faced folded metallic nanorods are proposed as a light concentrator and far-field radiation enhancement. The physical dimension of FFR is designed on the basis of λ_{spp} for resonance. This proposed structure is distinguished from unique induced charge redistribution, called "horizontal dual dipoles and vertical dual dipoles". Due to the unique induced charge redistribution, plasmonic faced folded nanorods provide semi-circular surface current paths in visible range and enhanced far-field radiation intensity without regard to the incident polarization state of light. To experimentally verify the optical response of FFR unit, three-dimensional holographic microscopy is employed. Furthermore, more functionality of FFR unit is validated. Not only the enhanced radiating light field but also light concentration in the vicinity of z = 2 μm is found.

Current issue about the diffraction limit in a subwavelength region can be handled with plasmonic nanostructures using induced charge redistribution mechanism. In attempt to

find out the solution in raised agenda, metallic nanoislands are embedded inside a metallic nanoslit. Here, a metallic rectangular nanostructure is selected as a metallic nanoisland because of limitation in fabrication. Its dimension is optimally designed in visible range. Typically, a metallic nanoslit suffers from weak transmission caused by the conventional diffraction limit. To overcome the diffraction limit, metallic nanoislands are employed, expecting to give rise to plasmonic effect. When a metallic nanoisland is placed inside a metallic nanoslit on the incidence of horizontally-polarized light, anti-symmetric plasmonic waveguide mode from an embedded metallic nanoisalnd is generated in a proposed geometry. Meanwhile, when a metallic nanoisland is embedded in a metallic nanoslit on the incidence of vertically-polarized light, symmetric plasmonic waveguide mode is produced. These plasmonic modes with regard to the incident polarization state of light are also attributed to increase the transmitted light intensity, which is measured by near-field scanning optical microscopy and far-field scattering microscopy. Without regard to the incident polarization state of light, the transmitted light intensity is enhanced when metallic nanoislands are embedded in a metallic nanoslit. The degree of transmitted light intensity is associated with the number and spacing distance of embedded metallic nanoislands. Furthermore, embedded metallic nanoislands can tune the resonant wavelength in a whole structure. Although the resonance of a metallic nanoslit is very weak or cannot be observed, embedding metallic nanoislands can contribute to give rise to its own resonance. Hence, the resonant wavelength of the proposed structure is nearly similar to the resonant wavelength of a metallic nanoisland. The number of embedded nanoislands is directly associated with the resonance properties. It also insinuates that embedded metallic rectangular nanoisland can act as a charge relocator, SPP source, and resonance shifter in a metallic nanoslit. Therefore, this approach to overcome weak transmission passing through a metallic nanoslit and tune the resonance condition is numerically and experimentally proved and can resolve the aforementioned nanophotonic issue.

According to this dissertation, proposed new structures and approaches can be helpful to development of novel photonic and plasmonic devices such as biosensors and optical data storage.

APPENDIX

To supplement Chapter 3, three-dimensional reconstructed map emanating from the FFR unit placed in square aperture is presented here.

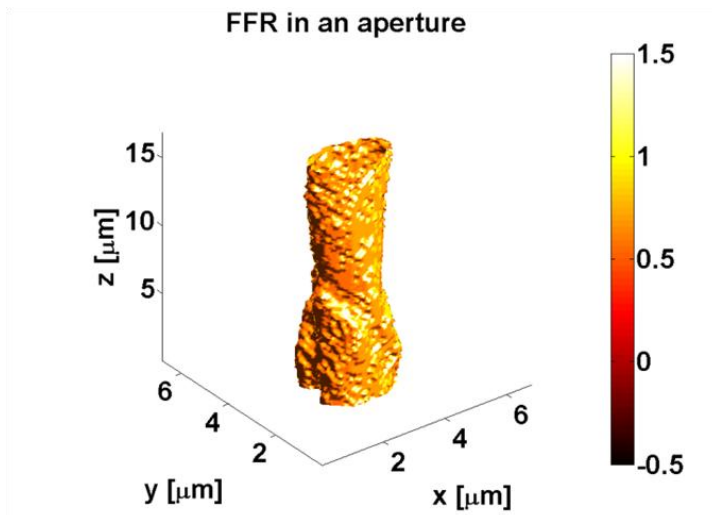

Figure A1. Three-dimensional reconstructed map emanating from FFR unit placed in square aperture.

As the supplementary images, the progress of light concentration through the FFR unit placed in square aperture is shown in Fig. A1. At z = 0.5 μm, diffraction arisen from the square aperture is observed. However, radiating light is concentrated in the vicinity of z = 2 μm. At z = 5 μm, radiating light is spread and very weak in Fig. A2.

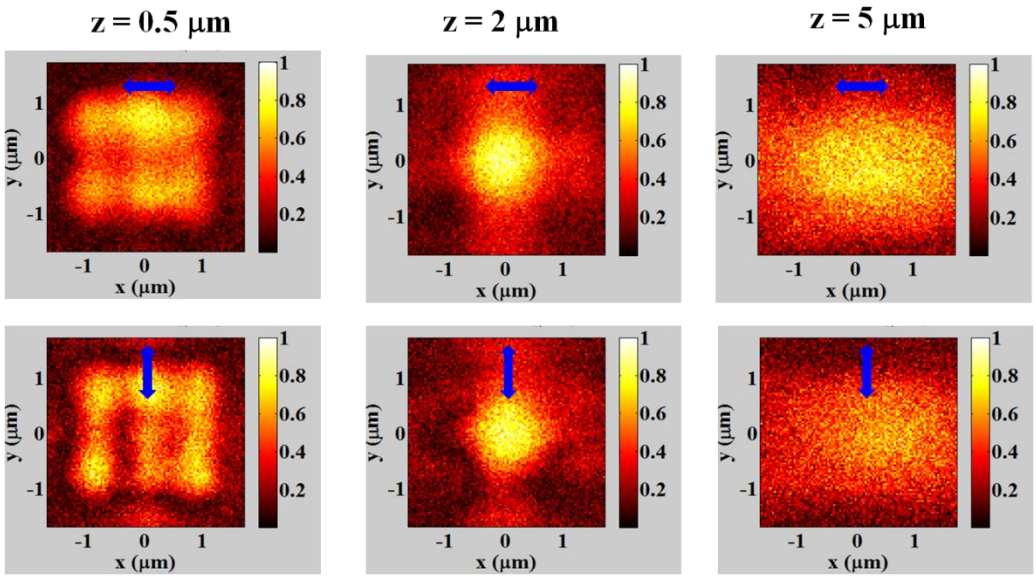

Figure A2. Cross-sectional views of transmitted light through an FFR unit at longitudinal (*z*) positions.

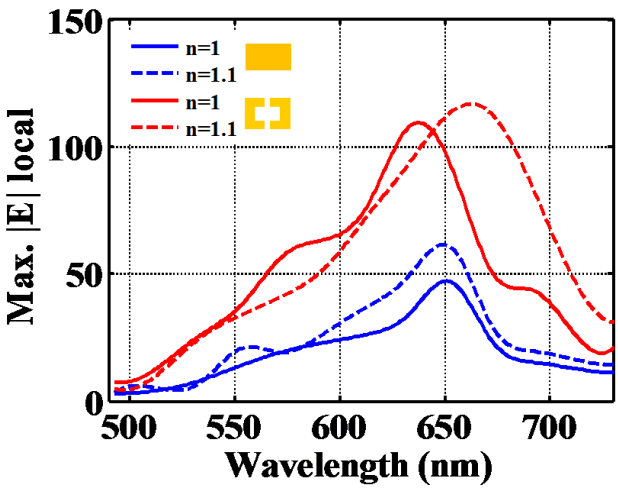

Figure A3. Spectra in response to the variation of surrounded bulk refractive index with respect to a metallic rectangular nanostructure and plasmonic faced folded metallic nanorods, respectively. Incident light is *x*-polarized and the magnitude of incident electric field is 1(V/m).

Previously, the unit of FFR is proposed as a light concentrator and experimentally demonstrated. FFR is uniquely taken account of localized, intense electromagnetic field

enhancement in near- and far-field region. It is also modeled by the horizontally dual-dipoles and vertically dual-dipoles with regard to the incident polarization state of light. Furthermore, extensive studies on plasmonic faced folded metallic nanorods are numerically performed. In Figure A3, the plasmonic sensing ability of FFR unit is numerically shown compared with the reference structure of a metallic rectangular nanostructure scaled by the same dimension. This figure indicates that FFR unit is more sensitive than a metallic rectangular nanostructure, responding to the variation of surrounded bulk refractive index. This phenomenon can result from both the highly localized field strength and confined capability caused by FFR unit. Hence, this property can be considered as one of the advantages observed in FFR unit.

Bibliography

1. L. Novotny and B. Hecht, Principles of Nano-optics (Cambridge University Press, 2006).
2. W.L. Barnes, A. Dereux, and T.W. Ebbesen, "Surface plasmon subwavelength optics," Nature **424**, 824-830 (2003).
3. C.Cong, W.C. Junus, Z. Shen, and T. Yu, "New colloidal lithographic nanopatterns fabricated by combining pre-heating and reactive ion etching," Nanoscale Res Lett. **4**, 1324-1328 (2009).
4. M.L. Brongersma and P.G. Kik, *Surface plasmon nanophotonics*. Springer, 2007.
5. E. Hutter and J.H. Fendler, "Exploitation of localized surface plasmon resonance," Advan. Mater. **16**, 1685-1706 (2004).
6. P.K. Jain, M.A. El-Sayed, "Plasmonic coupling in noble metal nanostructures," Chem. Phys. Lett. **487**, 153-164 (2010).
7. M.E. Stewart, C.R. Anderton, L.B. Thompson, J. Maria, S.K. Gray, J.A. Rogers, and R.G. Nuzzo, "Nanostructured plasmonic sensors," Chem. Rev. **108**, 494-521 (2008).
8. T. Vo-Dink, H.-N. Wang, and J. Scaffidi, "Plasmonic nanoprobes for SERS biosensing and bioimaing," J. Biophotonics **3**, 89-102 (2010).
9. L. Zhang, F.X. Gu, J.M. Chan, A.Z. Wang, R.S. Langer, and O.C. Farokhzad, "Nanoparticles in medicine: Therapeutic applications and developments," Clinical Pharm. & Therapeutics **83**, 761-769 (2008).
10. E. Cubukcu, E.A. Kort, K.B. Crozier, and F. Capasso, "Plasmonic laser antenna," Appl. Phys. Lett. **89**, 093120 (2006).
11. Q. H. Park, "Optical antennas and plasmonics," Contemp. Phys. **50**, 407-423 (2009).
12. E. Ozbay, "Plasmonics: Merging photonics and electronics at nanoscale dimensions," Science **311**, 189-193 (2006).

13. T. Pakizeh, M. Kall, “Unidirectional ultracompact optical nanoantennas,” Nano Lett. **9**, 2343-2349 (2009).
14. A.D. McFarland and R.P. Van Duyne, “Single silver nanoparticles as real-time optical sensors with zeptomole sensitivity, ” Nano Lett. **3**, 1057-1062 (2003).
15. K.S. Lee, and M.A. El-Sayed,“Gold and silver nanoparticles in sensing and imaging: Sensitivity of plasmon response to size, shape, and metal composition, ” J. Phys. Chem. B **110**, 19220-19225 (2006).
16. E.M. Larsson, J. Alegret, M. Kall, and D.S. Sutherland, “Sensing characteristics of NIR localized surface plasmon resonances in gold nanoring for application as ultrasensitive biosensors,” Nano Lett. **5**, 1256-1263 (2007).
17. R. Bukasov, T.A. Ali, P. Nordlander, and J.S. Shumaker-Parry, “Probing the plasmonic near-field of gold nanocrescent antennas,” ACS Nano **4**, 6639-6650 (2010).
18. S.K. Dondapati, T.K. Sau, C. Hrelescu, T.A. Klar, F.D. Stefani, and J. Feldmann, “Label-free biosensing based on single gold nanostars as plasmonic transducers,” ACS Nano **4**, 6318-6322 (2010).
19. Y. Fu, Y. Liu, X. Zhou, Z. Xu, and F. Fang, “Experimental investigationof superfocusing of plasmonic lens with chirped circular nanoslits,” Opt. Express **18**, 3438-3443 (2010).
20. T. Pakizeh and M. Kall, “Unidirectional ultracompact optical nanoantennas,” Nano Lett. **9**, 2343-2349 (2009).
21. T. Kosako, Y. Kadoya, and H.F. Hofmann, “Directional control of light by a nano-optical Yagi-Uda antenna,” Nat. Photonics **4**, 312-315 (2010).
22. E. Cubukcu, N. Yu, E.J. Smythe, L. Diehl, K.B. Crozier, and F. Capasso, “Plasmonic laser antennas and relateddevices,” IEEE J. Select. Top. Quantum Electron. **14**, 1448-1461 (2008).
23. J.H. Kang, D.S. Kim, and Q.-H. Park, “Local capacitor model forplasmonic electric field enhancement,” Phys. Rev. Lett., **102**, 093906-1-093906-4 (2009).
24. S. Maier, P. Kik, H. Atwater, S. Meltzer, E. Harel, B. Koel, and A. Requicha, “Local detection of electromagnetic energy transport below the diffraction limit

in metal nanoparticle plasmon waveguide, ” Nat. Mater., **2**, 229-232 (2003).

25. B. Liedberg, C. Nylander, and I. Lunstrom, “Surface plasmon resonance for gas detection and biosensing,” Sens.Actuat. **4**, 299-304 (1983).
26. T. Ebbesen, H. Lezec, H. Ghaemi, T. Thio, and P. Wolff, “Extraordinary optical transmission through subwavelength hole arrays,” Nature **391**, 667-669 (1998).
27. R.D. Grober, R.J. Schoelkopf, and D.E. Prober, “Optical antenna: Towards a unity efficiency near-field opticalprobe,” Appl. Phys. Lett. **70**, 1354-1356 (1997).
28. P.K. Jain, and M.A. El-Sayed, “Plasmonic coupling in nobel metal nanostructure, ” Chem. Phys. Lett. **487**, 153-164 (2010).
29. J. Zhu and F.-K. Li, “Effect of aspect ratio on the inter-surface plasmonic coupling of tubular gold nanoparticle, ” Eur. Phys. J. B **80**, 83-87 (2011).
30. P.F. Liao and A. Wokaun, “Lightning rod effect in surface enhanced Raman scattering, ” J. Chem. Phys. **76**, 751-752 (1982).
31. T. Chung, S.-Y. Lee, E.Y. Song, H. Chun, and B. Lee, “Plasmonic nanostructures for nano-scale bio-sensing,” Sensors **11**, 10907-10929 (2011).
32. N. Vogel, J. Fischer, R. Mohammadi, M. Retsch, H.-J. Butt, K. Landfester, C.K. Weiss, and M. Kreiter, “Plasmon hybridization in stacked double crescents arrays fabricated by colloidal lithography,” Nano Lett. **11**, 446-454 (2011).
33. F. Hao, C.L. Nehl, J.H. Hafner, and P. Nordlander, “Plasmon resonances of a gold nanostar,” Nano Lett., **7**, 729-732 (2007).
34. C. Hrelescu, T.K. Sau, A.L. Rogach, F. Jackel, G. Laurent, L. Douillard, and F. Charra, “Selective excitation of individual plasmonic hotspots at the tips of single gold nanostars,” Nano Lett. **11**, 402-407 (2011).
35. S. Kim, Y. Lim, H. Kim, J. Park, and B. Lee, “Optical beam focusing by a single subwavelength metal slit surrounded by chirped dielectric surface gratings,” Appl. Phys. Lett. **92**, 013103 (2008).
36. S. Kim, H. Kim, Y. Lim, and B. Lee, “Off-axis directional beaming of optical field diffracted by a single subwavelength metal slit with asymmetric dielectric surface gratings,” Appl. Phys. Lett. **90**, 051113 (2007).

37. P. Muhlschlegel, H.J. Eisler, O.J.F. Martin, B. Hecht, and D.W. Pohl, "Resonant optical antennas," Science **308**, 1607-1609 (2005).
38. W. Stutzman and G. Thiele, Antenna Theory and Design, 2nd ed. (John Wiley & Sons, New York, 1998).
39. A.F. Oskooi, D. Roundy, M. Ibanescu, P. Bermel, J.D. Joannopoulos, and S.G. Johnson, "A flexible freesoftware package for electromagnetic simulations by the FDTD method," Comput. Phys. Commun. **181**, 687-702 (2010).
40. E. Palik, *Handboook of Optical Constant of Solids* (Academic, London, 1985).
41. J. Xu, T. Xu, J. Wang, and Q. Tian, "Design tips of nanoapertures with strong field enhancement and proposal of novel L-shaped aperture," Opt. Eng. **44**, 018001 (2004).
42. M. Born and E. Wolf, *Principles of Optics*, 7th ed. (Cambridge University Press, Cambridge, 1999).
43. S. Park, M. Pelton, M. Liu, P. Guyot-Sionnest, and N.F. Scherer, "Ultrafast resonant dynamics of surface plasmons in gold nanorods," J. Phys. Chem. C **111**, 116-123 (2007)
44. R.D. Murley, "Mie theory of light scattering - Limitations on accuracy of approximate methods of computation," J. Phys. Chem. 64, 161-162 (1960).
45. We can find almost the same response when the length of vertical rods is 430 nm, the same as the folded rods when *unfolded*.
46. Y. Lim, S.-Y. Lee, and B. Lee, "Transflective digital holographic microscopy and its use for probing plasmonic light beaming," Opt. Express **19**, 5202-5212 (2011).
47. Y. Lim, J. Hahn, S. Kim, J. Park, H. Kim, and B. Lee, "Plasmonic light beaming manipulation and its detection using holographic microscopy," IEEE J. Quantum Electron. **46**, 300-305 (2010).
48. J.W. Goodman, *Introduction to Fourier Optics*, 2nd ed. (McGraw-Hill, New York, 1996).
49. J. Hahn, H. Kim, S.-W. Cho, and B. Lee, "Phase-shifting interferometry with genetic algorithm-based twin image noise elimination," Appl. Opt. **47**, 4068-

4076 (2008).

50. D.F.P. Pile, T. Ogawa, D.K. Gramotnev, Y. Matsuzaki, K.C. Vernon, K. Yamaguchi, T. Okamoto, M. Haraguchi, and M. Fukui, "Two dimensionally localized modes of a nanoscale gap plasmon waveguide," Appl. Phys. Lett., **87**, 261114-1-261114-3 (2005).
51. Y. Fu, Y. Liu, X. Zhou, Z. Xu, and F. Fang, "Experimental investigation of superfocusing of plasmonic lens with chirped circular nanoslits," Opt. Express **18**, 3438-3443 (2010).
52. S. Collin, G. Vincent, R. Haidar, N. Bardou, S. Rommeluere, and J.-L. Pelouard, "Nearly perfect Fano transmission resonances through nanoslits drilled in a metallic membrane," Phys. Rev. Lett. **104**, 027401-1-027401-4 (2010).
53. C.M. Wang, H.I. Huang, C.C. Chao, J.Y. Chang, and Y. Sheng, "Transmission enhancement through a trench surrounded nano metallicslit by bump reactors," Opt. Express **15**, 3496-3501 (2007).
54. J.S. White, G. Veronis, Z. Yu, E.S. Barnard, A. Chandran, S. Fan, and M.L. Brongersma, "Extraordinary optical absorption through subwavelength slits," Opt. Lett. **34**, 686-688 (2009).
55. B. Lee, S. Kim, H. Kim, and Y. Lim, "The use of plasmonics in light beaming and focusing, " Prog. Quantum Electron. **34**, 47-87 (2010).
56. S.-Y. Lee, W. Lee, Y. Lee, J.-Y. Won, J. Kim, I.-M. Lee, and B. Lee, "Phase controlled directional switching of surface plasmon polaritons via beam interference," Laser Photon. Rev. **7**, 273-279 (2013).
57. L. Yin, V. Vlasko-Vlasov, J. Pearson, J. Hiller, J. Hua, U. Welp, D. Brown, and C. Kimball, "Subwavelength focusing and guiding of surface plasmons," Nano Lett. **5**, 1399-1402 (2005).
58. S.-Y. Lee, I.-M. Lee, J. Park, S. Oh, W. Lee, K.-Y. Kim, and B. Lee, "Role of magnetic induction currents in nanoslit excitationof surface plasmon polaritons," Phys. Rev. Lett. 108, 213907-1-213907-5 (2012).
59. G. Zhao, "THz transmission properties of metallic slit array," IEEE Trans.Terahertz Sci. Technol. **3**, 85-91 (2010).

60. B. Lee, I.-M. Lee, S. Kim, D.-H. Oh, and L. Hesselink, “Review on subwavelength confinement of light with plasmonics,” J. Modern Opt. **57**, 1479-1497 (2010).
61. Y. Xie, A.R. Zakharian, J.V. Moloney, and M. Mansuripur, “Transmissionof light through slit apertures in metallic films,” Opt. Exp **12**, 6106-6121 (2004).
62. T.H. Isaac, J. Gomez Rivas, J.R. Sambles, W.L. Barnes, and E. Hendry, “Surface plasmon mediated transmission of subwavelength slits at THz frequencies,” Phys. Rev. B **77**, 113411-1-113411-4 (2008).
63. Y. Pang, C. Genet, and T.W. Ebbesen, “Optical transmission through subwavelength slit apertures in metallic films,” Opt. Commun. **280**, 10-15 (2007).
64. H.-R. Park, Y.-M. Bahk, K.J. Ahn, Q.-H. Park, D.-S. Kim, L. Martin-Moreno, F.J. Garcia-Vidal, and J. Bravo-Abad, “Controlling terahertz radiation with nanoscale metal barriers embedded in nano slot antennas,” ACS Nano **5**, 8340-8345 (2011).
65. M.J. Kofke, D.H. Waldeck, and G.C. Walker, “Composite nanoparticle nanoslit arrays: A novel platform for LSPR mediated subwavelength optical transmission,” Opt. Exp. **18**, 7705-7713 (2010).
66. T. Chung, Y. Lim, I.-M. Lee, S.-Y. Lee, J. Choi, S. Roh, K.-Y. Kim, and B. Lee, “A compact light concentrator by the use of plasmonic faced folded nano-rods,” Opt. Exp. **19**, 20751-20760 (2011).
67. A.S. Marathay and J.F. McCalmont, “Vector diffraction theory for electromagnetic waves” J. Opt. Soc. Am. A **18**, 2585-2593 (2001).
68. A.M. Funston, C. Novo, T.J. Davis, and P. Mulvaney,“Plasmon coupling of gold nanorods at short distances and in different geometries,” Nano Lett. **9**, 1651-1658 (2009).
69. J.A. Schuller, E.S. Barnard, W. Cai, Y.C. Jun, J.S. White, and M.L. Brongersma, “Plasmonics for extreme light concentration and manipulation,” Nature Mater. **9**, 193-204 (2010).

한글 초록

금속-유전체 사이의 경계면을 통해 진행하는 표면 플라즈몬은 전자기파로서, 대부분의 에너지가 금속과 유전체 사이의 경계면 근처에서 회절 한계보다 좁은 영역에 집속된다. 입사 파장보다 작은 나노 금속물에 빛을 입사하면, 금속-유전체 사이에서 발생하는 표면 플라즈몬에 의한 전자기파 세기(intensity)의 증가로 인해, 광학적 안테나의 역할을 수행하거나 전자기파를 파장보다 작은 영역에 집속시키는 것이 가능해진다. 본 논문에서는 이러한 파장보다 작은 나노 금속 구조물을 마이크로파 영역의 안테나의 한 종류인 folded 다이폴 안테나와 비슷한 원리로 디자인한 faced folded 금속 나노 구조물을 제안하였다. 기존의 결합된 두개의 금속 막대 구조 또는 잘 알려진 보우-타이 금속 구조가 빛의 편광 방향에 대해 매우 민감하다는 단점을 가지고 있는 반면에, 제안된 이 구조는 빛의 편광 방향에 상관없이 집속 된 강한 전자기장의 세기를 갖는 특성을 보여준다.

더불어, faced folded 금속 나노 구조물을 마이크로파 영역의 folded 다이폴 안테나의 원리와 유사한 접근방법을 가지고 모델링하였다. 또한, 제안된 구조물의 특징으로서, folding 효과는 faced folded 금속 나노 구조물에 새로운 표면 전류분포를 유도함을 수치적 계산을 통해 확인하였다. 이러한 새로운 표면 전류 분포로 부터, 빛의 편광 방향에 상관없이 제안된 구조의 강한 집속 전기장 세기를 확인할 수 있었다. 제안된 구조물의 광학적 특성을 실험적으로 확인하기 위해, 삼차원 홀로그래픽 마이크로스코피를 통해 faced folded 금속나노 구조물에서 방사하는 삼차원 빛의 경로를 여러위치에서 확인 하였다. 실험결과를 통해, bare aperture 에 놓여있는 faced folded 금속 나노 구조물이 일반적인 bare aperture 에 비해 빛의 집결과 세기 증대에 기여함을 확인 하였다.

이러한 플라즈모닉 특성을 갖는 금속 나노 구조물들을 이용하여, 나노포토닉스 분야에 현존하는 기술적 이슈들을 해결하기 위한 시도가 광범위하게 이루어 지고 있다. 본 논문에서는 파장 이하의 금속 나노 슬릿이 가지고 있는 굴절한계에 따른 빛의 낮은 투과율을 극복하기 위하여 나노 슬릿 안에 금속 나노 구조물을 embedding 하는 것을 제안하였다. 이는 나노 슬릿 안에 금속 나노 구조물이 일종의 섬(island) 처럼 놓여 있는 것과 유사한 개념이다. Embedded 된 금속 나노 구조물에 의해 나노 슬릿이 가지고 있는 문제점인 빛의 낮은 투과율을 극복하는 것을 수치적, 실험적으로 확인할 수 있었다. 구체적으로, embedded 된 금속 나노 구조물이 입사된 빛의 편광 방향에 따라 플라즈모닉 도파로 모드를 유도하여, 나노 슬릿을 투과하는 빛의 세기 증대에 기여하게 된다. 또한, embedded 된 금속 나노 구조물의 갯수에 따라 스펙트럼에서 공진 파장을 조절되어지는것을 관찰하였다. 일반적인 금속 나노 슬릿은 특정한 공진 파장을 보여주고 있지 않다. Embedded 된 금속 나노 구조물의 갯수가 증가함에 따라 뚜렷한 공진 파장을 갖게 되는 것을 시뮬레이션을 통해 확인 하였다. 이는 embedded 된 금속 나노 구조물이 나노 슬릿안에서의 투과되는 빛의 공진 특성을 결정하는 역할을 수행한다는 것을 보이고 있다. 따라서, embedded 된 금속 나노 구조물들이 전체 나노 슬릿의 공진 조건과 투과되는 빛의 세기를 결정짓은 역할을 수행한다는 것을 수치적, 실험적으로 제안 및 관찰하였다.

결과적으로, 본 논문에서는 가시광 대역에서의 금속 나노 구조물의 구조적 디자인을 통해서 빛의 집결과 세기 증대를 기대할 수 있는 광학 안테나 구조를 제안하고 실험을 통해 검증하였다. 또한, 이러한 금속 나노 구조물들의 특성을 이용하여, 파장 이하 크기의 금속 나노 슬릿이 가지고 있는 문제점을 해결하기 위한 방법을 제시하였다.

감사의 글

박사 졸업 논문을 쓰기까지 많은 인연들이 있었고, 이루 헤아릴 수 없는 도움과 격려, 응원을 받았습니다. 그분들에게 이 짧은 글로나마 감사함을 전하고자 합니다.

먼저 저의 지도교수님이신 이병호 교수님께 존경과 감사의 말씀을 올립니다. 여러 가지로 부족한 저를 믿고 기회를 주셔서 감사합니다. 광학 분야에 무지한 저를 세심하게 지도해 주시고 이끌어 주셨기에 조금이나마 제가 발전해 나갈 수 있었습니다. 또한, 안팎으로 성실하고 열정적인 교수님의 모습에서 제자신을 반성하며 보다 더 나은 모습으로 성장해 나아가는 발판이 되었습니다.

바쁘신 와중에도 저의 박사논문을 심사해주신 이신두 교수님, 정윤찬 교수님, 유경식 교수님께도 깊이 감사드립니다. 보잘것 없는 저의 논문을 성심껏 지도해 주셔서 많은 것을 깨닫고 배울 수 있었습니다. 그리고 제가 연구실에 처음들어 왔을때부터 물심양면 저를 지도해 주시고 조언해 주신 김경염 교수님께도 깊은 감사의 말씀을 드립니다.

서울대학교에 박사과정을 들어오기 전에 저는 여러 곳에서 많은 은혜를 받았습니다. 학부때, 저를 아껴주시고 성심껏 여러장의 추천서를 써주신 경희대학교 이범선 교수님께 이제서야 감사의 말씀을 드릴 수 있게 되었습니다. 저의 첫번째 석사과정이었던 포항공대에서 저의 지도교수님이셨던, 이재구 교수님께도 감사의 말씀을 드립니다. 고요한 포항에서 연구하는 방법과 자세를 교수님을 통해 처음으로 배웠던 그 시절은 잊혀지지 않습니다. 아무것도 모르는 저를 미국 실리콘 밸리 Lam research 라는 세계적인 기업에 인턴으로 뽑아주신

손종원 박사님께도 갚지 못할 감사함을 가지고 있습니다. 그리고 엔지니어로서 처음으로 일한 직장, 삼성전자 반도체 연구소 공정개발팀의 홍진 박사님, 채윤숙 과장님, 그리고 풍부한 엔지니어링 마인드의 배인덕 선배님께 감사드립니다.

두번째 석사과정을 했던, Cornell 대학에서도 여러 교수님들의 격려와 도움을 받았습니다. 저의 지도교수님이셨던 Belina 교수님, 언제나 웃으시면서 저의 어려움을 자신의 일처럼 도와주신 점 잊지 않고 있습니다. 인생의 롤모델로 삼은 Hammer 교수님, 머릿속에 교수님 얼굴만 떠올려도 가슴이 뭉클해 집니다. 배운 사람으로써 사회에서 어떠한 자세로 어떠한 역할을 해야 하는지 교수님을 통해 느끼고 배울 수 있었습니다. 마음을 다해 감사드리며, 앞으로도 계속 잊지 않겠습니다.

서울대 OEQELAB에서 박사과정을 하면서도 참으로 감사한 인연들이 많았습니다. 많은 가르침과 도움을 주신 이일민 박사님과 임용준 박사님, 가장 먼저 만난 명석하고 성실한 정현이, 유쾌하면서도 섬세한 숙영이, 속 깊은 성우, 마음 따뜻한 영민이, 똑똑한 재현이, 다재다능한 지수, 산같이 높아보이는 세윤이, 모범적인 동호, 모두 졸업하고 떠났지만 항상 기억하며 고마운 마음입니다. 성실하고 또 성실하신 한식 선배님, 맥가이버 같은 준범이에게도 감사함을 전합니다. 그리고 같이 졸업하는 멋지고 감수성 풍부한 다운이, 매우 훌륭하면서도 언제나 겸손한 승열이에게도 고마움을 전합니다. 특히, 무지한 누나를 도와주느라 고생한 승열이에게는 여러가지로 많은 고마움을 가지고 있단다. 그리고 착하고 다부진 의영이, 자랑스러운 고등학교 후배 기훈이, 똑부러지면서도 친절한 지운이, 부드러우면서 강인한 순기, 항상 열심히 하는 Chen Ni, 대표 훈남 종현이, 그리고 플라즈모닉스 팀을 앞으로 이끌어 갈 규호, 규근, 현수, 준수, 재범이, 3D 팀을 이끌어 갈 영모, 종영, 창원이등 다 언급하지 못했지만 모두 좋은 인연으로 기억될 것입니다.

마지막으로, 저의 인생의 버팀목이 되어주는 가족들에게 사랑과 감사의 마음을 전하고자 합니다. 많은 어려움을 홀로 견뎌내시며 가족을 지키신 아버지, 그 곁을 인내로 견뎌내시며 고생하신 어머니께 깊이 감사드립니다. 항상 저를 응원하시는 할아버지, 드디어 할아버지 소원을 들어드려서 저도 기쁩니다. 그리고 부족한 점 많은 며느리에게 무한한 사랑과 지지를 해주신 아버님과 어머님께도 깊이 감사드립니다. 그리고 동생들 융경이 재흥이 에게도 고마움을 전합니다.

사랑스런 나의 보물, 현석이 현승이에게도 엄마의 고마운 마음을 전합니다. 항상 미안한 마음 뿐이지만, 현석이 현승이가 있기에 힘든 하루도 버텨 나갈 수 있었단다. 그리고, 여기까지 이끌어 준 나의 남편, 현석이 현승이 아빠에게 무한한 감사와 사랑의 마음을 전합니다. 말로 표현할 수 없을 만큼 깊고 넓은 사랑과 보살핌에 매일 매일 감동합니다. 아내로, 엄마로 살아갈 수 있게 해준 남편과 아이들덕에 저는 복이 많은 사람이라고 느끼고 있습니다.

제가 받은 것들에 감사하며, 이 사회에서 기여 할 수 있는 것이 무엇인가 항상 고민하며, 저의 아이들 그리고 아이들의 친구들이 살아갈 세상을 위해 해야 할 일을 찾아 끊임없이 노력하며 낮은 자세로 살아가겠습니다.

2014년 1월 정태린 올림.